Vietnam National University Ho Chi Minh City
University of Science
Faculty of Physics
Department of Theoretical Physics

ICISE, Quy Nhon, Vietnam
Institute For Interdisciplinary Research in Science and Education
Theoretical Physics Group

BACHELOR'S THESIS

Nguyen Tran Quang Thong

Scatterings of proton proton to leptons in the Standard Model

Supervisor: Dr. Le Duc Ninh.
Reviewer: Dr. Phan Hong Khiem

Ho Chi Minh City - 2019

Acknowledgement

It would not have been possible to write this thesis without help and support from the kindness of people around me, to only some of whom it is possible to give particular mention here.

First of all, I would like to express my sincere attitude to my supervisor, Dr. Le Duc Ninh for accepting me as his student and giving me an interesting topic to work with. The enthusiasm and patience of his instructions are the most important thing that helps me finish this thesis. His advice and motivation help me shape my path in High Energy Physics research career. During my time working with him, I learned not only valuable knowledge and skills but also the honest, integrity and hard-working attitude, which are crucial characteristics of a scientist.

I am grateful to Prof. Jean Tran Thanh Van for the tremendous support for my three-month staying at Institute For Interdisciplinary Research in Science and Education (IFIRSE) to work on the main part of my thesis.

For the staff member of IFIRSE, I would like to thanks Dr. Dao Thi Nhung and Assoc. Prof. Nguyen Thi Hong Van for their advice to deal with my thesis's problem.

I admire Dr. Phan Hong Khiem, my Quantum Field Theory and Particle Physics teacher, for accepted as my reviewer. He is the one that shows me the beauty of Particle Physics Phenomenology, that later becomes my passion. In every physical discussion, I have learned from him the simple ways to attack physical problems. Thanks, thay Khiem!

I am grateful to Dr. Vu Quang Tuyen, my Condensed Matter Physics and Computational Physics teacher for his lessons that taught me C++ coding skills and key lessons in numerical solutions. He is also teaching me how to live my life slowly and enjoy every of its.

I also would like to thank you all my teachers at the Department of Theoretical Physics: Dr. Vo Quoc Phong, Dr. Nguyen Huu Nha, Dr. Nguyen Ha Hung Chuong, Assoc. Prof. Nguyen Quoc Khanh and thay Dang Ngoc Chau through their lectures I have gained a lot of knowledge and valuable lessons.

For the 24th Vietnam School of Physics (VSOP24), I would like to thanks for all the lecturers: Prof. Dr. Margarete Mühlleitner for her motivation speech in Standard Model lecture, Prof. Dr. Gudrun Heinrich for the QCD calculations, Prof. Dr. Shin-Shan "Eiko" Yu for the particle physics experiments description at the LHC. I also appreciate the help from Prof. Dr. Misao Sasaki for the brilliant General Relativity lecture in the 6th Vietnam School of Astrophysics (VSOA6) and the amusing lecture of Prof. Dr. Boris Kayser about Neutrino Oscillation in the 2nd Vietnam School

in Neutrinos (VSON2). All of them was making my last summer truly a wonderful adventure into the physics world.

For interesting discussions and help, I would like to thank all of my seniors: Nguyen Thanh Tien Dat, Nguyen Hoang Dai Nghia, Phan Vo Hong Minh, Chau Thien Nhan, Vu Ngoc Khanh, Nguyen Quoc Viet. Special thanks go to Vuong Pham Ngoc Hoa for many fruitful discussion about the Phase Space Integral, Luu Hoang Nhan for his LSZ Reduction formula explanation, Dam Quang Nam for his helping with my Python code and Tran Quang Loc for the amusing discussions and conversations during the time I work with him at IFIRSE.

Last, but by no means least, I owe a great debt to my family: my mother Tran Thi To Quynh, my aunt Tran Thi To Uyen, my grandfather and grandmother Tran Si Chau and Nguyen Thi Ngai, my "brother from another mother" Chau Anh Khoa and my future wife Le Minh Ngoc, for their invaluable and unconditional support. They are the motivation for me to work hard, to become a successful physicist in the future.

Ho Chi Minh City, June 20, 2019
Nguyen Tran Quang Thong

Contents

List of Figures

List of Tables

Introduction

The Large Hadron Collider (LHC), which was built by the European Organization for Nuclear Research (CERN), is the most powerful particle collider. Its total collision energy of 13 TeV is not only a good condition to search for new particles, but also to study more deeply about the properties of discovered particles, such as the $W^{\pm}$ and Z bosons.

In this thesis, based on the Standard Model (SM) and the Parton Distribution Functions (PDF), we calculate the cross section of $pp \longrightarrow N$ leptons scattering processes inside the LHC at 13 TeV, with $N = 2, 4$. The Feynman amplitudes are calculated using the helicity amplitude method. The cross sections and kinematical distributions are calculated by using the Monte Carlo integration method for the case of $N = 2$. For the case $N = 4$, we present results at the amplitude level for the production of $e^+\nu_e\mu^+\mu^-$. Finally, we use Madgraph and MadAnalysis programs (Ref. [2]) to cross check our results at leading order.

This thesis is presented in the following chapters:

- **Chapter 1: The Standard Model**
  We give an overview of the Standard Model: the elementary particles and the Lagrangian. From there, we will calculate some Feynman rules (vertices and propagators), which will be used in later calculations.

- **Chapter 2: Collision of two partons into N leptons**
  Next, we will discuss the N-body phase space integral and give some master equations for the cases $N = 2, 4$. The parton distribution functions are also discussed and their application in proton-proton scatterings is introduced. This is needed for our later calculations in Chapter 3.

- **Chapter 3: Two-lepton production**
  In this chapter, we will apply the Monte Carlo method to calculate the cross section of $pp \longrightarrow e^+\nu_e + X$ and $pp \longrightarrow \mu^+\mu^- + X$ processes. This method also enables us to calculate the polar-angle and transverse-momentum distributions of a final-state particle. We then compare them with the results of the Madgraph and MadAnalysis.

- **Chapter 4: Process $pp \longrightarrow e^+\nu_e\mu^+\mu^- + X$**
  In this final chapter, we calculate all helicity amplitudes for the process $pp \longrightarrow e^+\nu_e\mu^+\mu^- + X$. The results will be compared against Madgraph.

Finally, conclusion and outlook will be presented.

Chapter 1

The Standard Model

1.1 An overview of Standard Model

The Standard Model is the particular physical model which summaries our present knowledge of the elementary particles's propeties and their behavior. It is able to describe three of four fundamental interactions: electromagnetic, weak and strong interactions. Gravity interaction is not considered in this model. Based on the framework of Quantum Field Theory and group theory, it is invariant under the local gauge transformations with the symmetry group $SU(3)_C \otimes SU(2)_L \otimes U(1)_Y$. The color group $SU(3)_C$ stands for the strong interaction, and the $SU(2)_L \otimes U(1)_Y$ is for the electroweak interaction spontaneously broken by the Higgs mechanism. In the Standard Model, the elementary particles can be classified like this table below:

Standard Model of Elementary Particles					
Fermions				Gauge Bosons	Higgs Boson
Quarks	u	c	t	g	H
	d	s	b	γ	
Leptons	ν_e	ν_μ	ν_τ	$W^\pm$	
	e	μ	τ	Z	
	I	**II**	**III**	Three generation of fermions	

Table 1.1: Classification of elementary particles in the SM, according to Ref. [1].

According to the SM, the gauge bosons $W^\pm$, Z, accquire masses through Higgs mechanism while the fermions gain masses with the help of gauge-invariant Yukawa interactions and Higg field. In the SM, the neutrinos are considered as massless and right-handed neutrinos are not introduced.

1.2 Lagrangian

The classical Lagrangian of SM, according to Ref. [3], can be expressed explicit by:

$$\begin{aligned}\mathcal{L}_{SM} = &-\frac{1}{4}G^A_{\mu\nu}G^{A,\mu\nu} - \frac{1}{4}W^I_{\mu\nu}W^{I,\mu\nu} - \frac{1}{4}B_{\mu\nu}B^{\mu\nu} \\ &+ \Big(D_\mu\phi\Big)^\dagger\Big(D^\mu\phi\Big) - \Big[-\mu^2\phi^\dagger\phi + \frac{\lambda}{2}(\phi^\dagger\phi)^2\Big] \\ &+ i\Big(\overline{l_L}\not{D}l_L + \overline{e_R}\not{D}e_R + \overline{q_L}\not{D}q_L + \overline{u_R}\not{D}u_R + \overline{d_R}\not{D}d_R\Big) \\ &- \Big(\overline{l_L}\Gamma_e e_R\phi + \overline{q_L}\Gamma_u u_R\tilde{\phi} + \overline{q_L}\Gamma_d d_R\phi + h.c\Big).\end{aligned} \tag{1.2.1}$$

The covariant derivative, according to Yang-Mills theory, have the form of:

$$D_\mu = \partial_\mu + ig_s\tau^A G^A_\mu + ig_2\tau^I W^I_\mu + ig_1 Y B_\mu, \tag{1.2.2}$$

where the generators of $SU(3)$ and $SU(2)$ group:

$$\begin{aligned}\tau^A &= \frac{1}{2}\lambda^A, \qquad \lambda^A\text{: Gell-Mann matrices,} \\ \tau^I &= \frac{1}{2}\sigma^I, \qquad \sigma^I\text{: Pauli matrices.}\end{aligned}$$

The $\Gamma_{e,u,d}$, which stands for the Yukawa couplings, are the 3×3 matrices in generation space. The notation Y stands for the weak hypercharge, which have the relation between the electric charge Q and the weak isospin I_3 of any particles by the Gell-Mann - Nishijima formula:

$$Q = I_3 + \frac{1}{2}Y, \tag{1.2.3}$$

and their values is list in Table 1.2 amd Table 1.3.

Fermion family	Left-chiral spinor				Right-chiral spinor			
		Electric charge Q	Weak isospin I_3	Weal hypercharge Y		Electric charge Q	Weak isospin I_3	Weak hypercharge Y
Leptons	ν_e, ν_μ, ν_τ	0	$+\frac{1}{2}$	-1	No interaction, if extant			
	e^-, μ^-, τ^-	-1	$-\frac{1}{2}$	-1	e^-_R, μ^-_R, τ^-_R	-1	0	-2
Quarks	u, c, t	$+\frac{2}{3}$	$+\frac{1}{2}$	$+\frac{1}{3}$	u_R, c_R, t_R	$+\frac{2}{3}$	0	$+\frac{4}{3}$
	d, s, b	$-\frac{1}{3}$	$-\frac{1}{2}$	$+\frac{1}{3}$	d_R, s_R, b_R	$-\frac{1}{3}$	0	$-\frac{2}{3}$

Table 1.2: Electric charges, weak isospin and weak hypercharge of quarks and leptons.

The field strengh tensor are given by:

$$\begin{cases} G^A_{\mu\nu} &= \partial_\mu G^A_\nu - \partial_\nu G^A_\mu - g_s f^{ABC}G^B_\mu G^C_\nu, \\ W^I_{\mu\nu} &= \partial_\mu W^I_\nu - \partial_\nu W^I_\mu - g_2\epsilon^{IJK}W^J_\mu W^K_\nu, \\ B_{\mu\nu} &= \partial_\mu B_\nu - \partial_\nu B_\mu. \end{cases} \tag{1.2.4}$$

Mediated fundamental interaction	Boson	Electric charge Q	Weak isospin I_3	Weak hypercharge Y
Weak	W	± 1	± 1	0
	Z	0	0	0
Electric	γ	0	0	0
Higgs	H^0	0	$-\frac{1}{2}$	$+1$

Table 1.3: Electric charges, weak isospin and weak hypercharges of some bosons.

The physical gauge fields can appears in the Lagrangian by the transformation from weak eigenstates to mass eigenstates as follow:

$$W_\mu^\pm = \frac{1}{\sqrt{2}}\Big(W_\mu^1 \mp W_\mu^2\Big), \tag{1.2.5}$$

$$\begin{pmatrix} Z_\mu \\ A_\mu \end{pmatrix} = \begin{pmatrix} \cos\theta_W & \sin\theta_W \\ -\sin\theta_W & \cos\theta_W \end{pmatrix} \begin{pmatrix} W_\mu^3 \\ B_\mu \end{pmatrix} = \begin{pmatrix} c_W & s_W \\ -s_W & c_W \end{pmatrix} \begin{pmatrix} W_\mu^3 \\ B_\mu \end{pmatrix}, \tag{1.2.6}$$

where θ_W is the Weinberg angle, which has:

$$\tan\theta_W = t_W = \frac{g_1}{g_2}. \tag{1.2.7}$$

1.3 Feynamn rules

From the lagrangian, we can have the Feynman rule to calculate the Feynman amplitude of any process. These feynman rule has been proved and compared with the results in Ref ¿ From the lagrangian, we can have Feynman rules to calculate the Feynman amplitudes of any process. These feynman rules have been proved and compared with the results in Ref. [4].

1.3.1 Vertex factors.

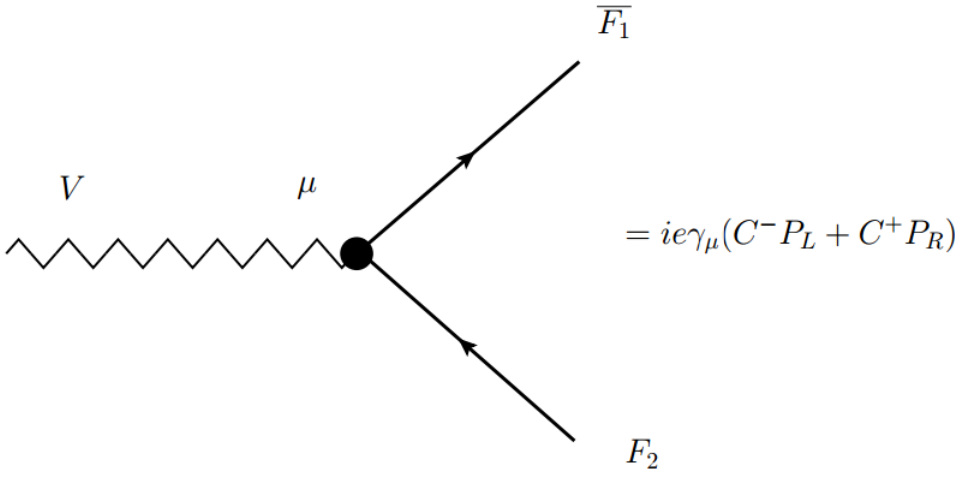

Figure 1.1: The vertex factor of VFF-coupling.

with the actual value of V, $\overline{F_1}$, F_2 and C^+, C^-:

$$\gamma\overline{f}_i f_j: \quad \begin{cases} C^+ &= -Q_f\delta_{ij} \\ C^- &= -Q_f\delta_{ij} \end{cases}, \qquad Z\overline{f}_i f_j: \quad \begin{cases} C^+ &= g_f^+\delta_{ij} \\ C^- &= g_f^-\delta_{ij} \end{cases}; \tag{1.3.8}$$

$$W^+\overline{u}_i d_j: \quad \begin{cases} C^+ &= 0 \\ C^- &= \frac{1}{\sqrt{2}s_W}\delta_{ij} \end{cases}, \qquad W^-\overline{d}_j u_i: \quad \begin{cases} C^+ &= 0 \\ C^- &= \frac{1}{\sqrt{2}s_W}\delta_{ij} \end{cases}; \tag{1.3.9}$$

$$W^+\overline{\nu_i} l_j: \quad \begin{cases} C^+ &= 0 \\ C^- &= \frac{1}{\sqrt{2}s_W}\delta_{ij} \end{cases}, \qquad W^-\bar{l}_j \nu_i: \quad \begin{cases} C^+ &= 0 \\ C^- &= \frac{1}{\sqrt{2}s_W}\delta_{ij} \end{cases}; \tag{1.3.10}$$

where:

$$g_f^+ = -\frac{s_W}{c_W}Q_f, \qquad g_f^- = \frac{I_3^f - s_W^2 Q_f}{s_W c_W}. \tag{1.3.11}$$

Then the explicit form of these VFF-vertices are:

$$\lambda^\mu_{\gamma\overline{f}f} = -ieQ_f\gamma^\mu, \tag{1.3.12}$$

$$\lambda^\mu_{Z\overline{f}f} = ie\gamma^\mu\frac{I_3(1-\gamma^5) - 2s_W^2 Q_f}{2s_W c_W}, \tag{1.3.13}$$

$$\lambda^\mu_{W\overline{F_1^i}F_2^j} = ie\gamma^\mu\frac{1}{\sqrt{2}s_W}P_L. \tag{1.3.14}$$

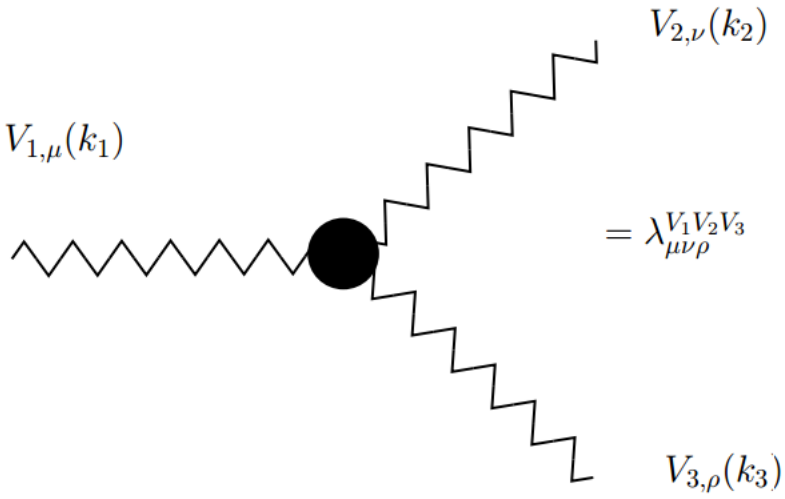

Figure 1.2: The 3-gauge bosons coupling.

The actual form of 3-gauge bosons vertex factor, with all the momenta are considered as incoming, is:

$$\lambda^{V_1V_2V_3}_{\mu\nu\rho} = -ieC\Big[g_{\mu\nu}(k_2-k_1)_\mu + g_{\nu\rho}(k_3-k_2)_\mu + g_{\rho\mu}(k_1-k_3)_\nu\Big], \tag{1.3.15}$$

with the actual values of V_1, V_2, V_3 and C are:

$$AW^+W^-: \quad C = 1, \tag{1.3.16}$$

$$ZW^+W^-: \quad C = -c_W/s_W. \tag{1.3.17}$$

1.3.2 Propagators

From the lagrangian, using equation of motion, we have these propagator for each gauge boson:

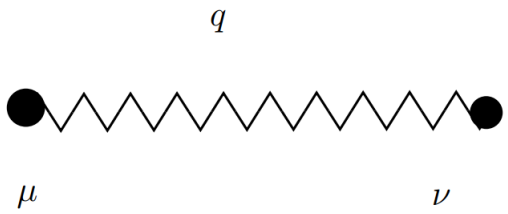

Figure 1.3: Vector boson propagator.

For each vector boson, their propagator are:

- Photon propagator:

$$D^A_{\mu\nu}(q) = -\frac{i}{q^2}\Big[g_{\mu\nu} - (1-\xi_A)\frac{q_\mu q_\nu}{q^2}\Big] \tag{1.3.18}$$

- $W^\pm$-boson propagators:

$$D^{W^\pm}_{\mu\nu}(q) = -\frac{i}{q^2-m_W^2}\Big[g_{\mu\nu} - (1-\xi_W)\frac{q_\mu q_\nu}{q^2-\xi_W m_W^2}\Big] \tag{1.3.19}$$

- Z-boson propagator:

$$D^Z_{\mu\nu}(q) = -\frac{i}{q^2 - m_Z^2}\left[g_{\mu\nu} - (1-\xi_Z)\frac{q_\mu q_\nu}{q^2 - \xi_Z m_Z^2}\right] \tag{1.3.20}$$

which ξ_A, ξ_W and ξ_Z are the gauge-fixing parameters.

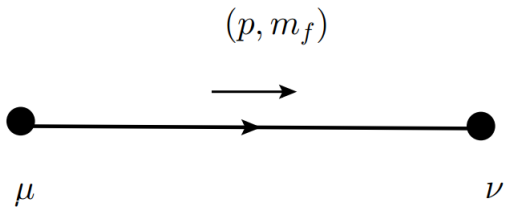

Figure 1.4: The fermion propagator.

The fermion propagtor, for the momenta has the same direction with the fermion line, is:

$$D_F = \frac{i(\not{p} + m_f)}{p^2 - m_f^2}. \tag{1.3.21}$$

Chapter 2

Collision of two partons into N leptons

Consider a collision between two partons (quarks) into leptons (the $2 \longrightarrow N$ process):

$$q_1(p_1, h_1) + \overline{q_2}(p_2, h_2) \longrightarrow \sum_{i=3}^{N+2, N\geq 1} \text{lepton}_i(p_i, h_i), \tag{2.0.1}$$

with p_i and h_i are the momentum and helicity parameter.

In this collision, the charge conservation and the energy conservation must be satisfied.

2.1 N-particle phase space

According to Ref. [5], the N-body phase space can be described as:

$$d\Omega_N = (2\pi)^4 \delta^{(4)}(P_i - P_f) \prod_{i=1}^{N} \frac{d^3 p_i}{(2\pi)^3 2E_i}, \tag{2.1.2}$$

with:

$$P_i: \text{ Sum of initial momenta,}$$
$$P_f: \text{ Sum of final momenta.}$$

Based on this formula, we can build the phase spaces for $2 \longrightarrow 2$ processes and $2 \longrightarrow 4$ process. All of their result had checked with Ref. [6].

2.1.1 2-body final state

Consider an $2 \longrightarrow 2$ process in the Partonic Center of Mass system (PCMs):

$$p_1 + p_2 \longrightarrow p_3 + p_4, \tag{2.1.3}$$

with $\mathbf{p}_1 = -\mathbf{p}_2$ and $\mathbf{p}_3 = -\mathbf{p}_4$, we have the invariance square mass:

$$s = (p_1 + p_2)^2 = (p_3 + p_4)^2. \tag{2.1.4}$$

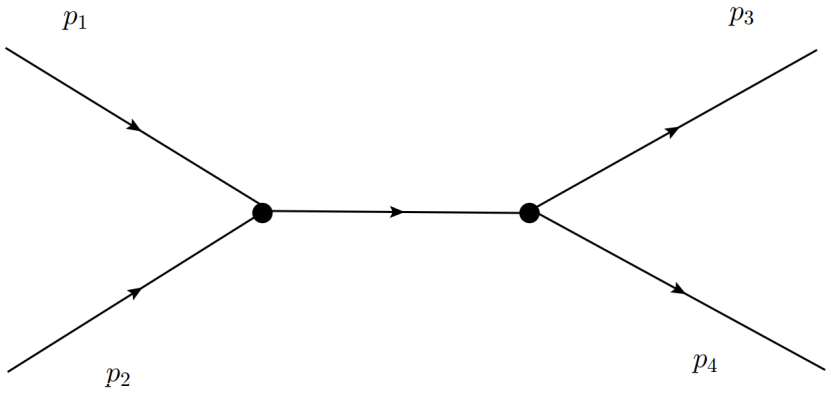

Figure 2.1: The $2 \longrightarrow 2$ process.

The phase space of 2-body final state is:

$$d\Omega_2 = \frac{d^3\mathbf{p}_3}{(2\pi)^3 2E_3}\frac{d^3\mathbf{p}_4}{(2\pi)^3 2E_4}(2\pi)^4\delta^4(p_1 + p_2 - p_3 - p_4). \tag{2.1.5}$$

After some transformation, which can be described specificly in Ref. [7], we have:

$$d\Omega_2 = \frac{1}{16\pi^2}d\cos\theta d\phi\frac{\lambda^{1/2}(s, m_3^2, m_4^2)}{2s}\theta(\sqrt{s} - m_3 - m_4), \tag{2.1.6}$$

with θ and ϕ are the polar and azimuthal angles of the p_3-particle. $\theta(\sqrt{s}-m_3-m_4)$ is the Heaviside function and $\lambda(s, m_3, m_4)$ is the Källén function, which has the definiton:

$$\lambda(a, b, c) = (a - b - c)^2 - 4bc. \tag{2.1.7}$$

From this result, we can calculate the 4-particles final state phase space.

2.1.2 4-body final state

Now, consider a $2 \longrightarrow 4$ process in the PCMs:

$$p_1 + p_2 \longrightarrow p_3 + p_4 + p_5 + p_6, \tag{2.1.8}$$

we have the phase space:

$$d\Omega_4 = \frac{d\mathbf{p}_3}{(2\pi)^3 2E_3}\frac{d^3\mathbf{p}_4}{(2\pi)^3 2E_4}\frac{d^3\mathbf{p}_5}{(2\pi)^3 2E_5}\frac{d^3\mathbf{p}_6}{(2\pi)^3 2E_6}(2\pi)^4\delta^4(p_1 + p_2 - \sum_{i=3}^{6} p_i). \tag{2.1.9}$$

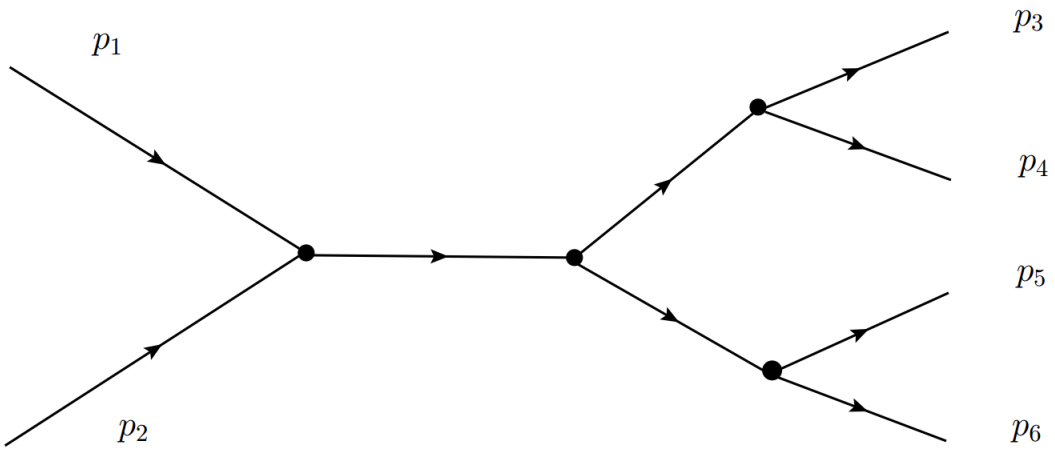

Figure 2.2: The $2 \longrightarrow 4$ process.

So, we can described this process by:

- In the PCMs:
$$p_1 + p_2 \longrightarrow p_{34} + p_{56} \tag{2.1.10}$$
- In the s_{34}-particle frame:
$$p_{34} \longrightarrow p_3 + p_4 \tag{2.1.11}$$
- In the s_{56}-particle frame:
$$p_{56} = p_5 + p_6 \tag{2.1.12}$$

Then the phase space can be rewriten as product of $2 \longrightarrow 2$ phase spaces:

$$d\Omega_4 = \frac{ds_{34}}{2\pi}\frac{ds_{56}}{2\pi} d\Omega_2(34,56) d\Omega_2(3,4) d\Omega_2(5,6). \tag{2.1.13}$$

After some transformation, we have:

$$\begin{aligned} d\Omega_4 =& \frac{ds_{34}}{2\pi}\frac{ds_{56}}{2\pi}\left[\frac{d\cos\theta d\phi}{4\pi^2}\frac{\lambda^{1/2}(s,s_{34},s_{56})}{8s}\right] \times \left[\frac{d\cos\theta_1 d\phi_1}{4\pi^2}\frac{\lambda^{1/2}(s_{34},m_3^2,m_4^2)}{8s_{34}}\right] \\ &\times \left[\frac{d\cos\theta_2 d\phi_2}{4\pi^2}\frac{\lambda^{1/2}(s_{56},m_5^2,m_6^2}{8s_{56}}\right], \end{aligned} \tag{2.1.14}$$

with the conditions:

$$\begin{aligned} (m_3+m_4)^2 \leq s_{34} \leq (\sqrt{s}-m_5-m_6)^2, \\ (m_5+m_6)^2 \leq s_{56} \leq (\sqrt{s}-\sqrt{s_{34}})^2. \end{aligned} \tag{2.1.15}$$

We have:

- θ and ϕ are the polar and azimuthal angles of s_{34}-particle in the PCMs.
- θ_1 and ϕ_1 are the polar and azimuthal of angles of p_3-particle in the s_{34}-particle rest frame.
- θ_2 and ϕ_2 are the polar and azimuthal of angles of p_5-particle in the s_{56}-particle rest frame.

2.2 Total cross section of parton-parton collision

The differential cross section is:

$$d\sigma_{2\longrightarrow N}^{parton} = \frac{1}{2E_1 2E_2|\mathbf{v}_1 - \mathbf{v}_2|} \times d\Omega_N \times |\mathcal{M}(p_1, p_2 \longrightarrow \sum_{i=1}^{N} p_i)|^2. \tag{2.2.16}$$

Consider the $2 \longrightarrow 2$ process, the total cross-section is:

$$\sigma_{2\longrightarrow 2}^{parton} = \frac{1}{2E_1 2E_2|\mathbf{v}_1 - \mathbf{v}_2|} \times \frac{1}{16\pi^2} \int_{-1}^{1} d\cos\theta \int_{0}^{2\pi} d\phi \frac{\lambda^{1/2}(s, m_3^2, m_4^2)}{2s} |\mathcal{M}(2 \to 2)|^2. \tag{2.2.17}$$

The total cross section of $2 \longrightarrow 4$ process is:

$$\begin{aligned}\sigma_{2\longrightarrow 4}^{parton} = \frac{1}{2E_1 2E_2|\mathbf{v}_1 - \mathbf{v}_2|} \times & \int_{(m_3+m_4)^2}^{(\sqrt{s}-m_5-m_6)^2} \frac{ds_{34}}{2\pi} \int_{m_5+m_6}^{(\sqrt{s}-\sqrt{s_{34}})^2} \frac{ds_{56}}{2\pi} \\ & \times \Big[\int_{-1}^{1} d\cos\theta \int_{0}^{2\pi} d\phi \frac{\lambda^{1/2}(s, s_{34}, s_{56})}{32\pi^2 s}\Big] \times \Big[\int_{-1}^{1} d\cos\theta_1 \int_{0}^{2\pi} d\phi_1 \frac{\lambda^{1/2}(s_{34}, m_3^2, m_4^2)}{32\pi^2 s_{34}}\Big] \\ & \times \Big[\int_{-1}^{1} d\cos\theta_2 \int_{0}^{2\pi} d\phi_2 \frac{\lambda^{1/2}(s_{56}, m_5^2, m_6^2}{8 s_{56}}\Big] |\mathcal{M}(2 \to 4)|^2.\end{aligned} \tag{2.2.18}$$

2.3 Proton-proton collision

2.3.1 Parton model and Parton Distribution Funcitons

The parton model, which was proposed by Richard Feynman in 1969, is a way to analyze high-energy hadron collision. According to this model, a hadron is composed of a number of point-like constituents, termed "partons". Later, with the experimental observation of **Bjorken scalling** (Ref. [8]), the validation of the quark model, and the confirmation of asymptotic freedom in quantum chromodynamics, partons were matched to **quarks** and **gluons**.

Therefore, we can consider a proton as:

$$\text{proton} = \Big\{u, d, c, s, b, g, \bar{u}, \bar{d}, \bar{c}, \bar{s}, \bar{b}\Big\}. \tag{2.3.19}$$

Because of the large mass, compared to other quarks, the top quark is not considered in this model, due to small probability to finding it in the proton.

A parton distribution function (pdf) within so called *collinear factorization* is defined as the probability density for finding a particle with a certain longitudinal momentum fraction x at resolution scale Q^2. Parton distribution functions are obtained by fitting observables to experimental data; they cannot be calculated using perturbative QCD.

Experimentally determined parton distribution functions are available from various groups worldwide. In this thesis, we using the **NNPDF_23_lo_as_0119_qed** from the NNPDF Collaboration as provided via the LHAPDF library version 6.2.1 (Ref. [9]).

2.3.2 Total cross section of proton-proton collision

Consider proton proton scattering with total collision energy at **13 TeV**. We have:

$$\sqrt{s} = 13 \quad (\text{TeV}) \Longrightarrow E = \frac{\sqrt{s}}{2} = 6500 \quad (\text{TeV}). \tag{2.3.20}$$

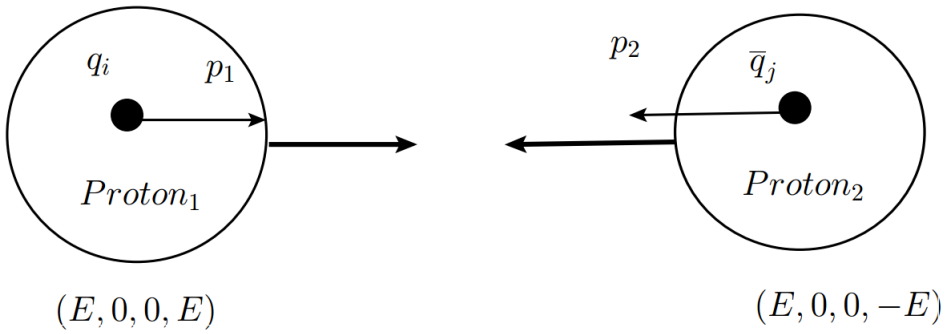

Figure 2.3: An example for proton-proton scattering.

Now, consider a parton in proton 1, with momentum p_1, collides with another parton in proton 2, with momentum p_2. In the Laboratory frame, these momentum are:

$$p_1 = (x_1 E, 0, 0, x_1 E), \tag{2.3.21}$$
$$p_2 = (x_2 E, 0, 0, -x_2 E), \tag{2.3.22}$$

with x_1 and x_2 are the momentum fraction of each particle inside the proton that contain it.

Then, in the partonic center of mass frame:

$$s_p = (p_1 + p_2)^2 = x_1 x_2 s. \tag{2.3.23}$$

Therefore, the probaility density $pdf(id, x, Q^2)$ for a parton that contribute in this collision have the momentum fraction x, is depend on that fraction, the exact identity of parton and the energy scale Q, which is called factorization scale. We used this particle number scheme (from Ref. [10]) to identified these particles:

Particle	$\bar{t}$	$\bar{b}$	$\bar{c}$	$\bar{s}$	$\bar{u}$	$\bar{d}$	g	d	u	s	c	b	t
Id number (id)	-6	-5	-4	-3	-2	-1	0	1	2	3	4	5	6

Table 2.1: The particle number scheme using in LHAPDF set.

For every momentum in the laboratory frame, we have the total cross section for the $2 \longrightarrow 2$ and $2 \longrightarrow 4$ processes as:

$$\begin{aligned}\sigma^{pp}_{2\to 2} = &\sum_{id_1,id_2}\int_0^1 dx_1 \times pdf(x_1,id_1,Q^2)\int_0^1 dx_2 \times pdf(x_2,id_2,Q^2)\\ &\times\frac{1}{2E_1 2E_2|\mathbf{v}_1-\mathbf{v}_2|}\times\frac{1}{16\pi^2}\int_{-1}^1 d\cos\theta\int_0^{2\pi}d\phi\frac{\lambda^{1/2}(s,m_3^2,m_4^2)}{2s}|\mathcal{M}(2\to 2)|^2,\end{aligned} \tag{2.3.24}$$

$$\begin{aligned}\sigma^{pp}_{2\to 4} = &\sum_{id_1,id_2}\int_0^1 dx_1 \times pdf(x_1,id_1,Q^2)\int_0^1 dx_2 \times pdf(x_2,id_2,Q^2)\\ &\times\frac{1}{2E_1 2E_2|\mathbf{v}_1-\mathbf{v}_2|}\times\int_{(m_3+m_4)^2}^{(\sqrt{s}-m_5-m_6)^2}\frac{ds_{34}}{2\pi}\int_{m_5+m_6}^{(\sqrt{s}-\sqrt{s_{34}})^2}\frac{ds_{56}}{2\pi}\\ &\times\Big[\int_{-1}^1 d\cos\theta\int_0^{2\pi}d\phi\frac{\lambda^{1/2}(s,s_{34},s_{56})}{32\pi^2 s}\Big]\times\Big[\int_{-1}^1 d\cos\theta_1\int_0^{2\pi}d\phi_1\frac{\lambda^{1/2}(s_{34},m_3^2,m_4^2)}{32\pi^2 s_{34}}\Big]\\ &\times\Big[\int_{-1}^1 d\cos\theta_2\int_0^{2\pi}d\phi_2\frac{\lambda^{1/2}(s_{56},m_5^2,m_6^2}{8s_{56}}\Big]|\mathcal{M}(2\to 4)|^2.\end{aligned} \tag{2.3.25}$$

These equations are essential for the cross section calculation, using the Monte Carlo method. From their results we can find the kinematical distributions.

For the cross section distribution by polar angle, we have:

$$\begin{aligned}\frac{d\sigma^{pp}_{2\to 2}}{d\theta} = &\sum_{id_1,id_2}\int_0^1 dx_1 \times pdf(x_1,id_1,Q^2)\int_0^1 dx_2 \times pdf(x_2,id_2,Q^2)\\ &\times\frac{1}{2E_1 2E_2|\mathbf{v}_1-\mathbf{v}_2|}\times\frac{1}{16\pi^2}\int_0^{2\pi}d\phi\frac{\lambda^{1/2}(s,m_3^2,m_4^2)}{2s}|\mathcal{M}(2\to 2)|^2\sin\theta,\end{aligned} \tag{2.3.26}$$

Another necessary distribution is the transverse momentum distribution. We can accquire this quantities by switching from angular distribution to transverse momentum distribution, the transformation formular is given by

$$p_T = \sum_i p_T(\theta_i)\mathcal{J}_i = \sum_i p_T(\theta_i)\frac{d\theta}{dp_T(\theta)}\Big|_{\theta=\theta_i}. \tag{2.3.27}$$

Beside, for the transverse momentum, we still have:

$$p_T = |\vec{p}|\sin\theta \Longrightarrow \begin{cases}\theta_1 &= \arcsin(p_T/|\vec{p}|),\\ \theta_2 &= \pi-\arcsin(p_T/|\vec{p}|).\end{cases} \tag{2.3.28}$$

Here we have introduced the factor $\mathcal{J}_i$ which called Jacobian, the explicit form is:

$$\begin{aligned} \Big|\frac{d\theta}{dp_T}\Big| &= \frac{1}{|\vec{p}||\cos\theta|} = \frac{1}{|\vec{p}|\sqrt{1-\sin^2\theta}}, \\ \Longrightarrow \Big|\frac{d\theta}{dp_T}|_{\theta=\theta_1}\Big| &= \Big|\frac{d\theta}{dp_T}|_{\theta=\theta_2}\Big| = \frac{1}{\sqrt{|\vec{p}|^2-p_T^2}}. \end{aligned} \tag{2.3.29}$$

Then we have the distribution:

$$\begin{aligned} \frac{d\sigma^{pp}_{2\to2}}{dp_T} &= \sum_i \frac{d\sigma^{pp}_{2\to2}}{d\theta}|_{\theta=\theta_i}\Big|\frac{d\theta}{dp_T}|_{\theta=\theta_i}\Big| \\ &= \sum_{i=1}^{2}\sum_{id_1,id_2}\int_0^1 dx_1 \times pdf(x_1,id_1,Q^2)\int_0^1 dx_2 \times pdf(x_2,id_2,Q^2) \\ &\times \frac{1}{2E_1 2E_2|\mathbf{v}_1-\mathbf{v}_2|}\times\frac{1}{16\pi^2}\int_0^{2\pi} d\phi \frac{\lambda^{1/2}(s,m_3^2,m_4^2)}{2s}|\mathcal{M}(2\to2)|^2\frac{\sin\theta_i}{\sqrt{|\vec{p}|^2-p_T^2}} \\ &= \sum_{id_1,id_2}\int_0^1 dx_1 \times pdf(x_1,id_1,Q^2)\int_0^1 dx_2 \times pdf(x_2,id_2,Q^2) \\ &\times \frac{1}{2E_1 E_2|\mathbf{v}_1-\mathbf{v}_2|}\times\frac{1}{16\pi^2}\int_0^{2\pi} d\phi \frac{\lambda^{1/2}(s,m_3^2,m_4^2)}{2s}|\mathcal{M}(2\to2)|^2\frac{\sin\theta}{\sqrt{|\vec{p}|^2-p_T^2}} \end{aligned} \tag{2.3.30}$$

These integrals are calculated by using the Monte Carlo method. Because the appearance of the W and Z boson propagators, the squared amplitudes will have the Breit-Wigner functions. To make the errors descease, we can use the important sampling method, which is described in section C.2.

Chapter 3

Two-lepton production

We used the input parameters in Ref. [11] for later results comparison and update:

- Fermi constant:
$$G_F = 1.16637 \times 10^{-5}\ \text{GeV}^{-2} \tag{3.0.1}$$
- $W^{\pm}$-boson mass:
$$M_W = 80.385\ \text{GeV} \tag{3.0.2}$$
- $W^{\pm}$-boson decay width:
$$\Gamma_W = 2.085\ \text{GeV} \tag{3.0.3}$$
- Z-boson mass:
$$M_Z = 91.1876\ \text{GeV} \tag{3.0.4}$$
- Z-boson decay width:
$$\Gamma_Z = 2.4952\ \text{GeV} \tag{3.0.5}$$

All the fermions (except top-quark) are considered massless in the following calculation.

The top-quark's PDF is neglected.

3.1 Process $pp \longrightarrow e^+\nu_e + X$

First, we consider the scattering:
$$pp \longrightarrow e^+\nu_e + X. \tag{3.1.6}$$

In this process, X stands for the combination of jets and other composite particles: baryon and meson, that have the total electric charge as $+1$ to satisfy the conservation law.

In this collision, we only consider the two partonic-processes:
$$u + \bar{d} \longrightarrow e^+ + \nu_e, \tag{3.1.7}$$
$$c + \bar{s} \longrightarrow e^+ + \nu_e. \tag{3.1.8}$$

Due to the small value of the Cabibbo–Kobayashi–Maskawa matrix elements between two quarks with diffent generation, we neglect the $u\bar{s}$, $u\bar{b}$, $c\bar{d}$ and $c\bar{b}$ collisions.

3.1.1 Helicity amplitudes

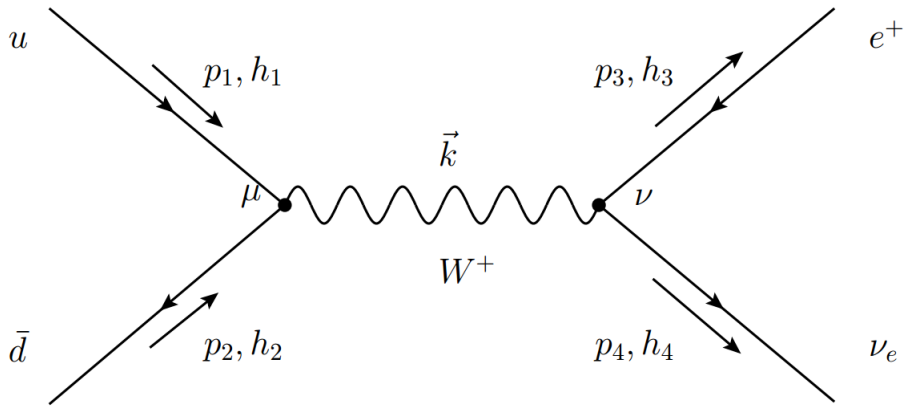

Figure 3.1: The $u + \bar{d} \longrightarrow e^+ + \nu_e$ process.

The $c\bar{s} \longrightarrow e^+\nu_e$ process have the same diagram like 3.1.

Based on this diagram, we have the feynman amplitudes:

$$\begin{aligned}\mathcal{M}_{u\bar{d}} &= \Big[\bar{v}(p_2,h_2)\lambda^{\mu}_{W^+u\bar{d}}u(p_1,h_1)\Big]D^{W^+}_{\mu\nu}(k)\Big[\bar{u}(p_4,h_4)\lambda^{\nu}_{W^+e^+\nu_e}v(p_3,h_3)\Big] \\ &= \Big[\bar{v}(p_2,h_2)ie\gamma^{\mu}\frac{1}{\sqrt{2}s_W}P_Lu(p_1,h_1)\Big]\Big[\bar{u}(p_4,h_4)ie\gamma^{\nu}\frac{1}{\sqrt{2}s_W}P_Lv(p_3,h_3)\Big] \\ &\times \frac{-i}{q^2-m_W^2+iM_W\Gamma_W}\Big[g_{\mu\nu}-(1-\xi_W)\frac{q_\mu q_\nu}{q^2-\xi_W m_W^2}\Big],\end{aligned} \tag{3.1.9}$$

$$\mathcal{M}_{\bar{d}u} = \mathcal{M}_{ud}\Big\{p_1 \longleftrightarrow p_2\Big\}, \tag{3.1.10}$$

$$\mathcal{M}_{c\bar{s}} = \mathcal{M}_{u\bar{d}}; \quad \mathcal{M}_{\bar{s}c} = \mathcal{M}_{\bar{d}u}. \tag{3.1.11}$$

3.1.2 Cross section

We have the total cross section:

$$\begin{aligned}\sigma^{pp}_{e^+\nu_e} &= \int_0^1 dx_1 \int_0^1 dx_2 \frac{1}{2E_1 2E_2|\mathbf{v}_1-\mathbf{v}_2|} \times \frac{1}{16\pi^2}\int_{-1}^{1} d\cos\theta \int_0^{2\pi} d\phi \times \frac{\lambda^{1/2}(s_p,0,0)}{2s_p} \\ &\times \sum_{id=2}^{3}\Big[pdf(x_1,id,m_W^2)pdf(x_2,1-id,M_W^2)|\mathcal{M}_{u\bar{d}}|^2 + pdf(x_1,1-id,m_W^2)pdf(x_2,id,m_W^2)|\mathcal{M}_{\bar{d}u}|^2\Big].\end{aligned} \tag{3.1.12}$$

In the experement at LHC, only the e^+ can be measured by the detectors (The neutrinos can't be detected). Also, for the small value of θ, the events can't be detected, due to the fact that you can't place detectors at small polar angles. The e^+ can't be detected also if their transverse

momentum is too low.

To avoid that, in our calculation we apply cuts on the transverse momentum of e^+ ($p_{T,e}$) and pseudo-rapidity (η_e). In this thesis, we consider ATLAS cuts (Ref. [12]) for the Monte Carlo integration:

$$\begin{cases} p_{T,e} & \geq 20 \text{ GeV}, \\ |\eta_e| & < 2.5, \end{cases} \tag{3.1.13}$$

where their definition are:

$$p_{T,e} = \sqrt{p_x^2 + p_y^2}, \tag{3.1.14}$$

$$\eta_e = -\ln\left[\tan\left(\frac{\theta}{2}\right)\right]. \tag{3.1.15}$$

Using the Monte Carlo method with 4×10^6 events, we have the result:

$$\sigma^{pp}_{e^+\nu_e} = 4467 \pm 34 \text{ pb}. \tag{3.1.16}$$

We can compare our result with the Madgraph program:

	C^{++} code	Madgraph
$\sigma^{pp}_{e^+\nu_e}$ (pb)	4467	4418
$\delta\sigma$ (pb)	34	4

Table 3.1: Cross section comparason between our C^{++} and Madgraph of $pp \longrightarrow e^+\nu_e + X$

The total error between two calculation is:

$$\delta\sigma = \sqrt{\delta\sigma^2_{C^{++}} + \delta\sigma^2_{Madgraph}} \approx 34.23 \text{ pb}. \tag{3.1.17}$$

Then we have:

$$\frac{|\sigma_{C^{++}} - \sigma_{Madgraph}|}{\delta\sigma} \approx 1.4. \tag{3.1.18}$$

Our result agreed with Madgraph with 1.4 σ.

3.1.3 Kinematical distributions

The Monte Carlo method, not only can used in integration, but also to calculated distributions.

From the data generated in the phase space, we can include them into 50 bins. Each bin contain the information, which is the range of the event minimum and maximum values.

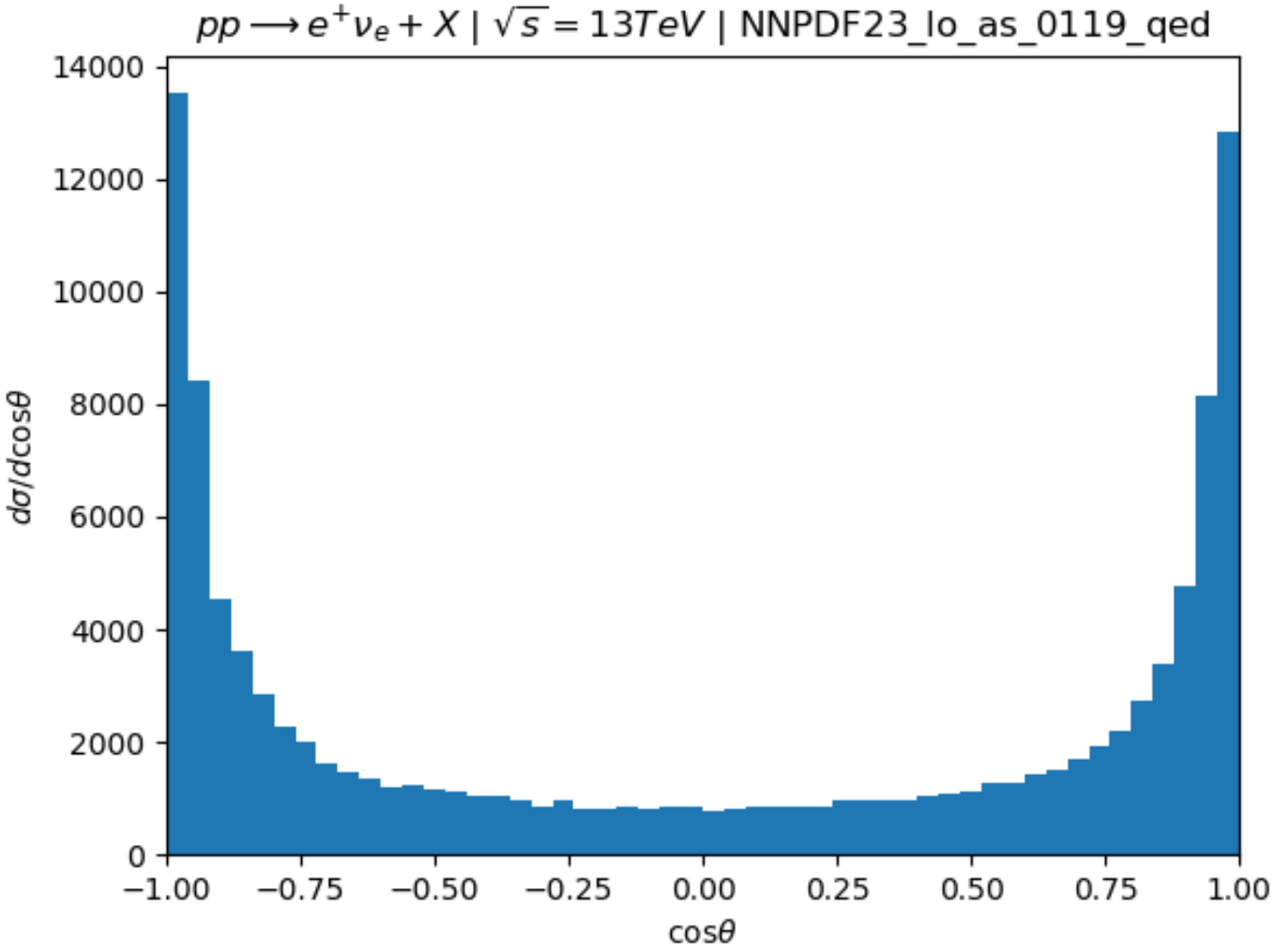

Figure 3.2: Cross section distribution by $\cos\theta$ of positron.

From figure.3.2, we can see that the e^+ is more likely to be detected near $\theta = 0$ and $\theta = \pi$, and the probability is smallest at $\theta = \pi/2$. The histogram is symmetric, which is true due to the fact that two proton beams have equal energy.

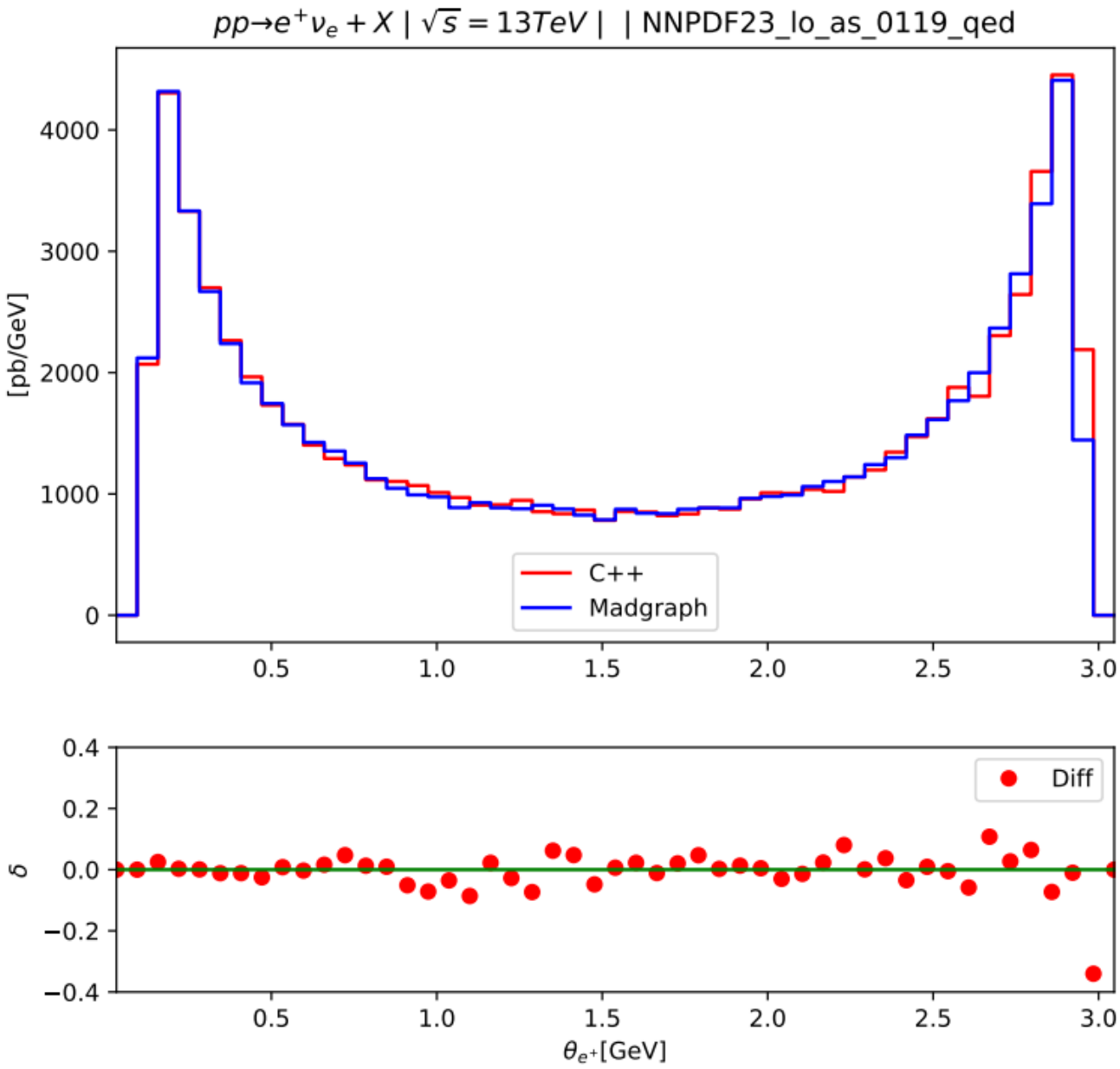

Figure 3.3: Cross section distribution by polar angle of positron with C++ code and Madgraph calculation

The **Diff** in Figure 3.3 is calculated as:

$$\textbf{Diff}(x) = \left(\frac{d\sigma^{pp}_{e^+\nu_e}}{dx}\Big|_{Madgraph} - \frac{d\sigma^{pp}_{e^+\nu_e}}{dx}\Big|_{C++}\right) \Big/ \frac{d\sigma^{pp}_{e^+\nu_e}}{dx}\Big|_{C++} \tag{3.1.19}$$

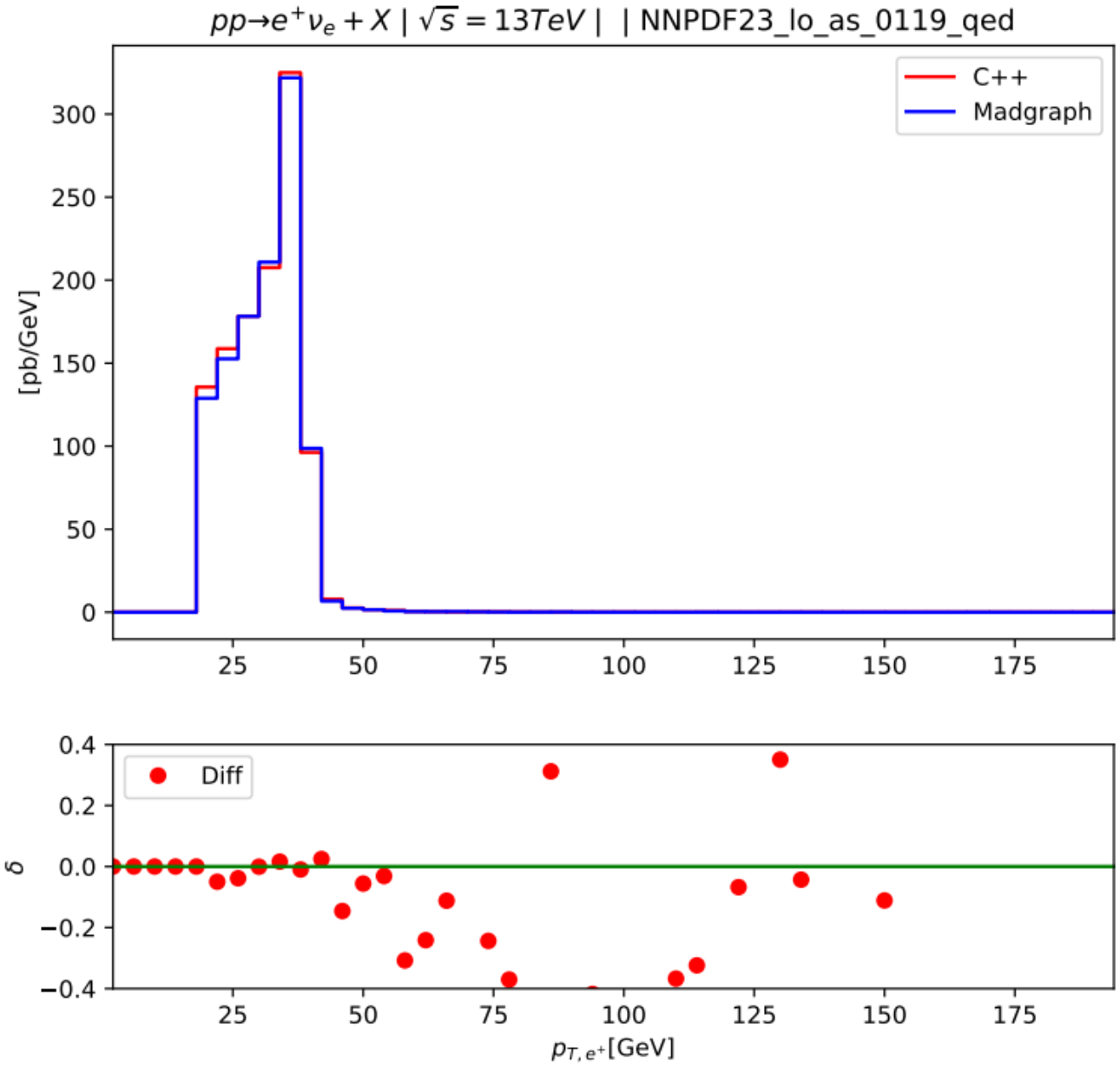

Figure 3.4: Cross section distribution by transverse momenta of positron.

3.2 Process $pp \longrightarrow \mu^+\mu^- + X$

Consider the scattering:

$$pp \longrightarrow \mu^+\mu^- + X. \tag{3.2.20}$$

In this process, X must have the electric charge $Q_X = +2$.

In this collision, neglect the top-quark, we have:

$$q_i + \bar{q} \longrightarrow \mu^+ + \mu^-, \tag{3.2.21}$$

which

$$q_i = \Big\{u, d, c, s, b\Big\}. \tag{3.2.22}$$

3.2.1 Helicity amplitudes

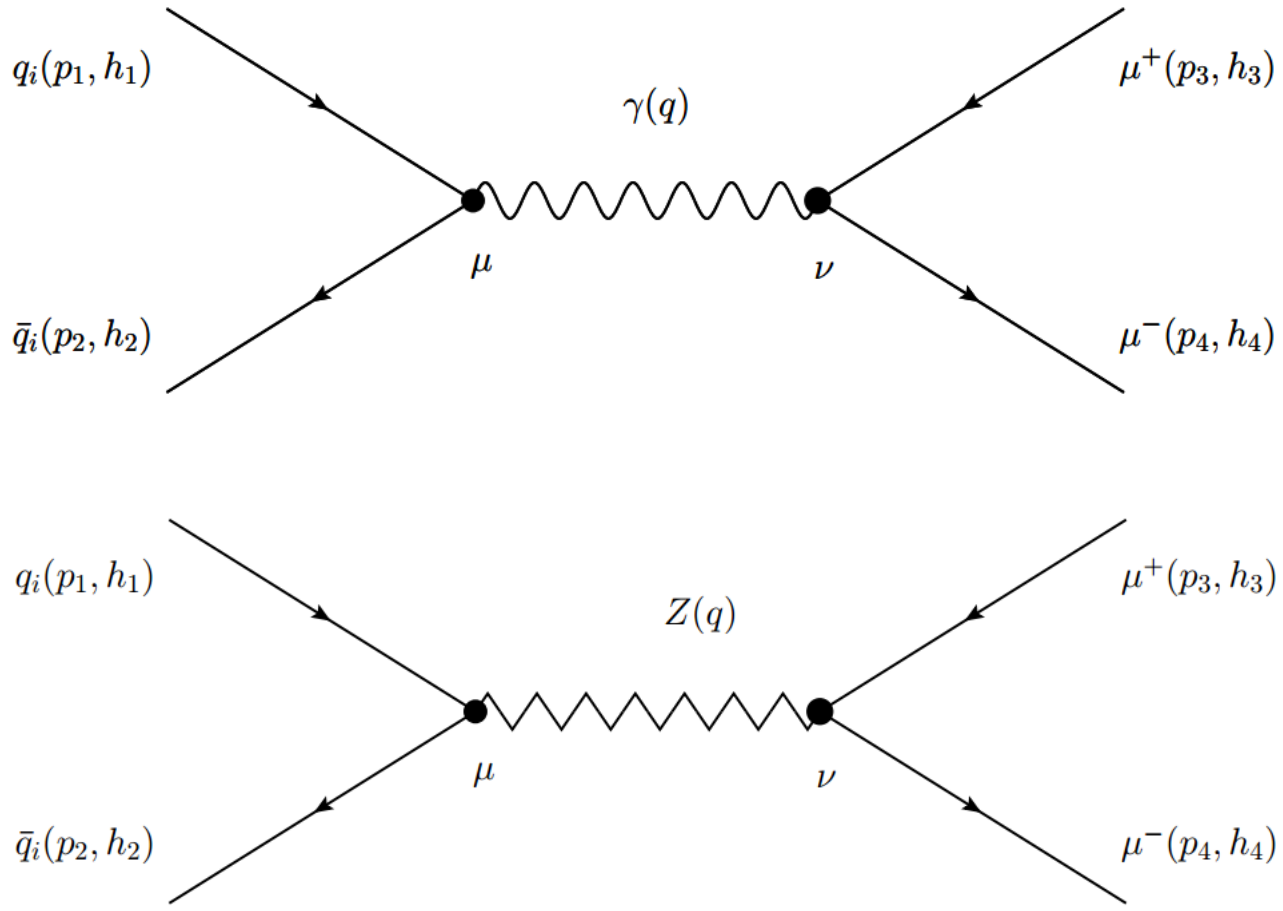

Figure 3.5: Feynman diagrams for $\bar{q}_i q_i \longrightarrow \mu^+\mu^-$.

Based on these diagrams, we have the Feynman amplitudes:

$$\begin{aligned}
\mathcal{M}^Z_{q_i\bar{q}_i} &= \Big[\bar{v}(p_2, h_2)\lambda^{\mu}_{Z\bar{q}_i q_i} u(p_1, h_1)\Big] D^Z_{\mu\nu}(q) \Big[\bar{u}(p_4, h_4)\lambda^{\nu}_{Z\mu^+\mu^-} v(p_3, h_3)\Big] \\
&= \left[\bar{v}(p_2, h_2) ie\gamma^{\mu} \frac{I_3^{q_i}(1-\gamma^5) - 2s_W^2 Q_{q_i}}{2s_W c_W} u(p_1, h_1)\right] \\
&\times \left[\bar{u}(p_4, h_4) \frac{I_3^{\mu}(1-\gamma^5) - 2s_W^2 Q_{\mu}}{2s_W c_W} v(p_3, h_3)\right] \\
&\times \frac{-i}{q^2 - m_Z^2 + iM_Z\Gamma_Z}\left[g_{\mu\nu} - (1-\xi_Z)\frac{q_\mu q_\nu}{q^2 - \xi_Z m_Z^2}\right],
\end{aligned} \tag{3.2.23}$$

$$\begin{aligned}\mathcal{M}^A_{q_i\bar{q}_i} &= \Big[\bar{v}(p_2,h_2)\lambda^{\mu}_{A\bar{q}_iq_i}u(p_1,h_1)\Big]D^A_{\mu\nu}(q)\Big[\bar{u}(p_4,h_4)\lambda^{\nu}_{A\mu^+\mu^-}v(p_3,h_3)\Big] \\ &= \Big[\bar{v}(p_2,h_2)(-ieQ_{q_i}\gamma^{\mu})u(p_1,h_1)\Big]\Big[\bar{u}(p_4,h_4)(-ieQ_{\mu}\gamma^{\nu})v(p_3,h_3)\Big] \\ &\times \frac{-i}{q^2}\Big[g_{\mu\nu} - (1-\xi_A\frac{q_\mu q_\nu}{q^2}\Big].\end{aligned} \tag{3.2.24}$$

The total Feynman amplitude is:

$$\mathcal{M}_{q_i\bar{q}_i} = \mathcal{M}^A_{q_i\bar{q}_i} + \mathcal{M}^Z_{q_i\bar{q}_i}. \tag{3.2.25}$$

3.2.2 Cross section

We have the total cross section:

$$\begin{aligned}\sigma^{pp}_{\mu^+\mu^-} = &\int_0^1 dx_1 \int_0^1 dx_2 \frac{1}{2E_1 2E_2|\mathbf{v}_1-\mathbf{v}_2|} \times \frac{1}{16\pi^2}\int_{-1}^{1} d\cos\theta \int_0^{2\pi} d\phi \times \frac{\lambda^{1/2}(s_p,0,0)}{2s_p} \\ &\times \sum_{id=1}^{5}\Big[pdf(x_1,id,m_Z^2)pdf(x_2,-id,M_Z^2)|\mathcal{M}_{q_{id}\bar{q}_{id}}|^2 + pdf(x_1,-id,m_Z^2)pdf(x_2,id,m_Z^2)|\mathcal{M}_{\bar{q}_{id}q_{id}}|^2\Big].\end{aligned} \tag{3.2.26}$$

We used these cuts on μ^+ and μ^- particles for the calculation (Ref. [11]):

$$\begin{cases} p_{T,\mu^-} & \geq 15 \text{ GeV}, \\ |\eta_{\mu^-}| & < 2.5, \\ p_{T,\mu^+} & \geq 15 \text{ GeV}, \\ |\eta_{\mu^+}| & < 2.5, \\ 66.0 & < \sqrt{s_p} < 116.0 \text{ GeV}. \end{cases} \tag{3.2.27}$$

The additional cut $66.0 < \sqrt{s_p} < 116.0$ GeV is included to avoid the divergence when the invariant mass of the propagator is near zero, which is the collinear singularity when the photon propagator appears.

Using the Monte Carlo method with 4×10^6 events, we have the result:

$$\sigma^{pp}_{\mu^+\mu^-} = 565 \pm 2 \text{ pb}. \tag{3.2.28}$$

We can compare our result with the Madgraph program:

	C++ code	Madgraph
$\sigma^{pp}_{\mu^+\mu^-}$ (pb)	565	564
$\delta\sigma$ (pb)	2	1

Table 3.2: Cross section comparison between C++ and Madgraph of $pp \longrightarrow \mu^+\mu^- + X$.

The total error between two calculation is:

$$\delta\sigma = \sqrt{\delta\sigma_C^2 + \delta\sigma_{Madgraph}^2} \approx 2.24 \text{ pb}. \tag{3.2.29}$$

Then we have:

$$\frac{|\sigma_{C++} - \sigma_{Madgraph}|}{\delta\sigma} \approx 0.45. \tag{3.2.30}$$

Our result agreed with Madgraph within 0.45 σ.

3.2.3 Kinematical distributions

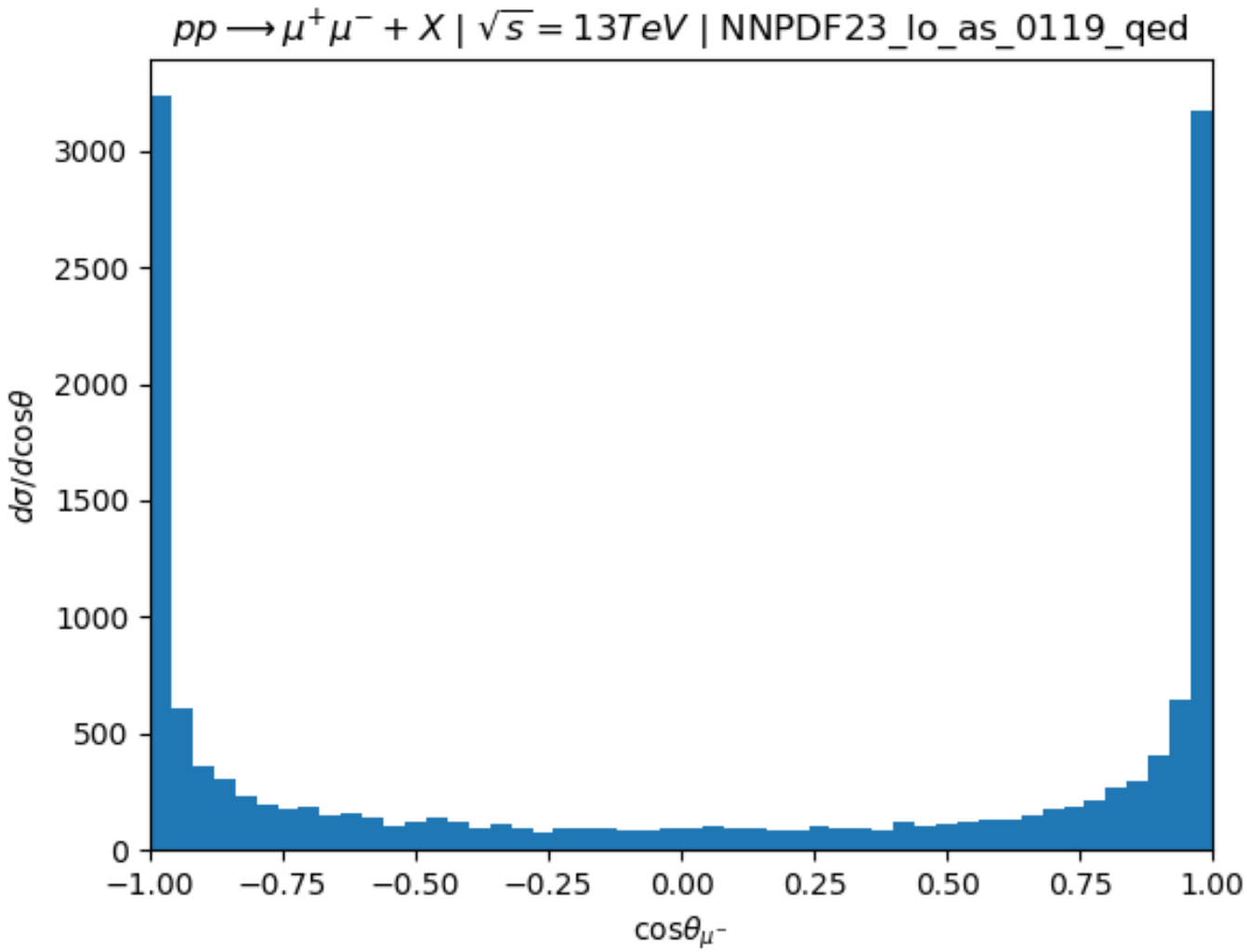

Figure 3.6: Cross section distribution by $\cos\theta$ of μ^-.

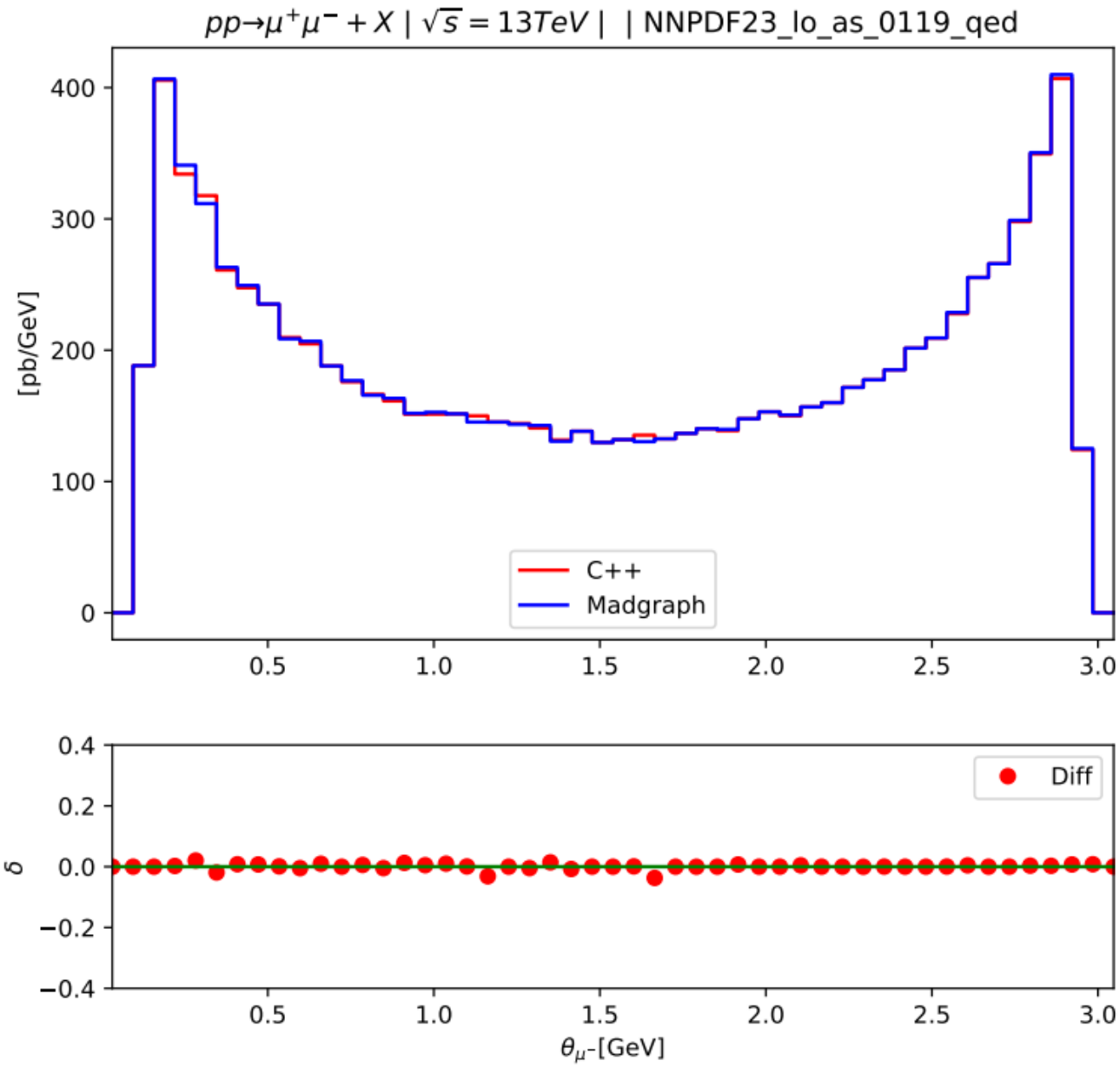

Figure 3.7: Cross section distribution by θ of μ^- of C++ code and Madgraph calculations. The subtiles figure is the different between two results.

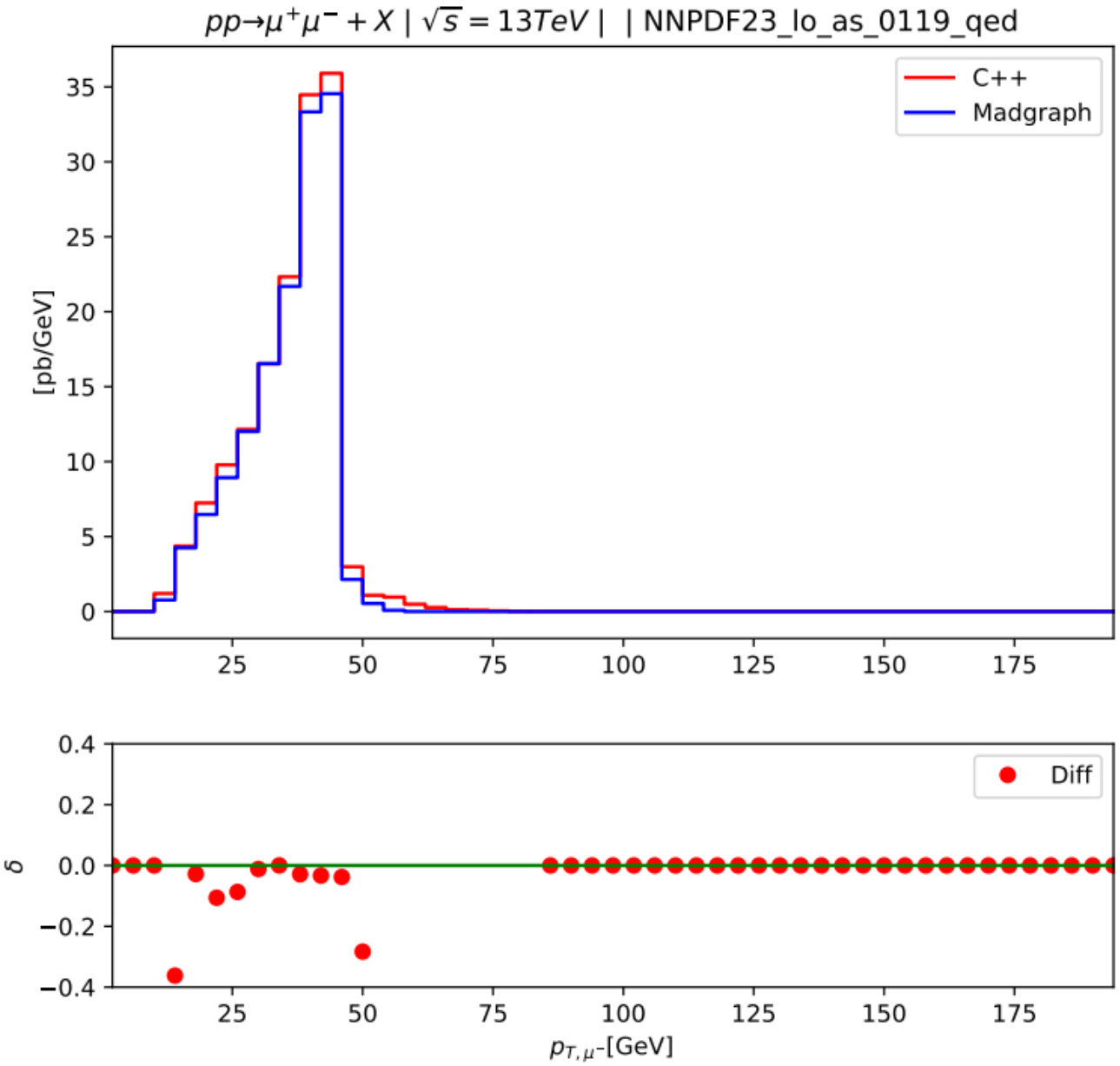

Figure 3.8: Cross section distribution by transverse momentum of μ^- of C++ code and Madgraph calculations. The subtiles figure is the different between two results.

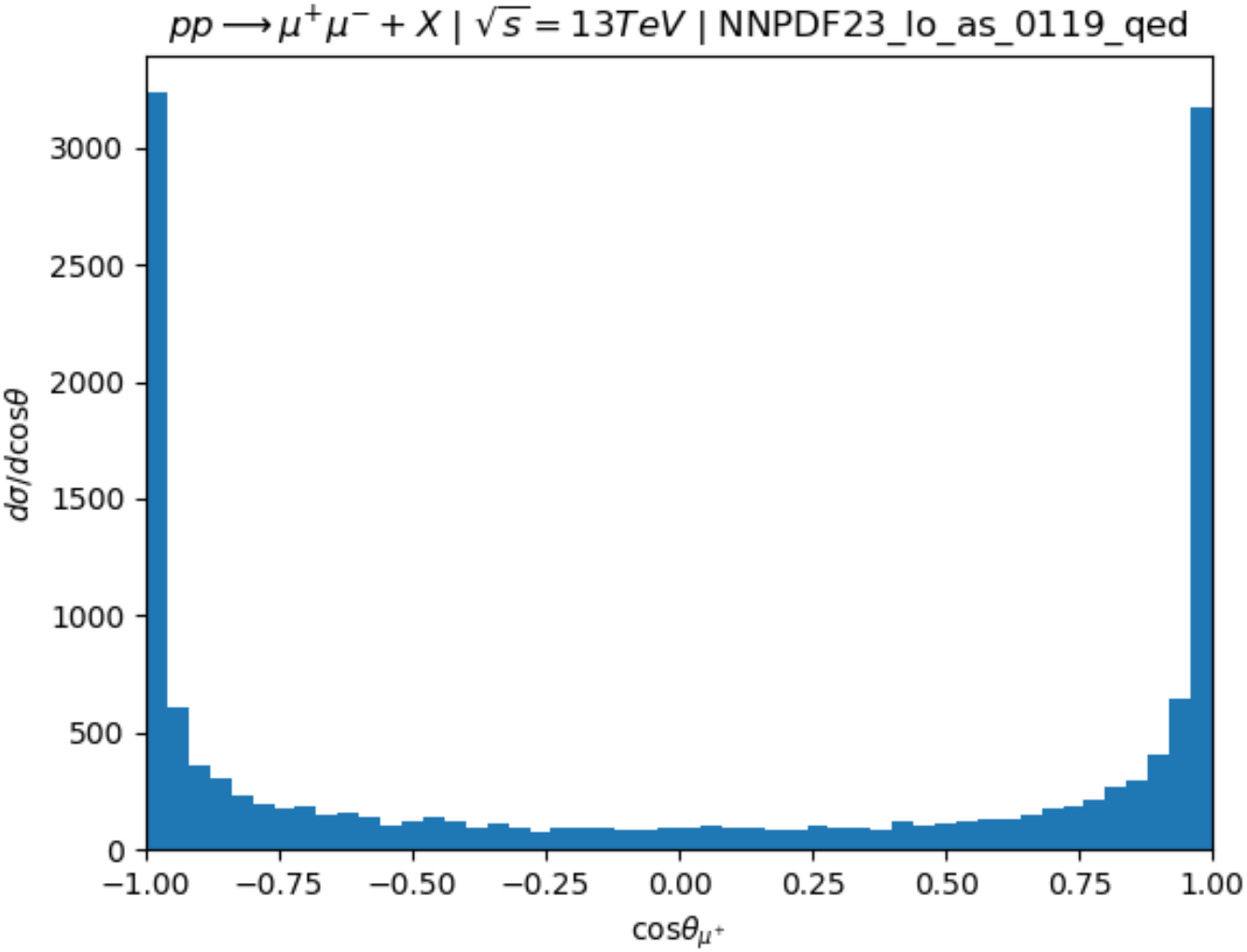

Figure 3.9: Cross section distribution by $\cos\theta$ of μ^-.

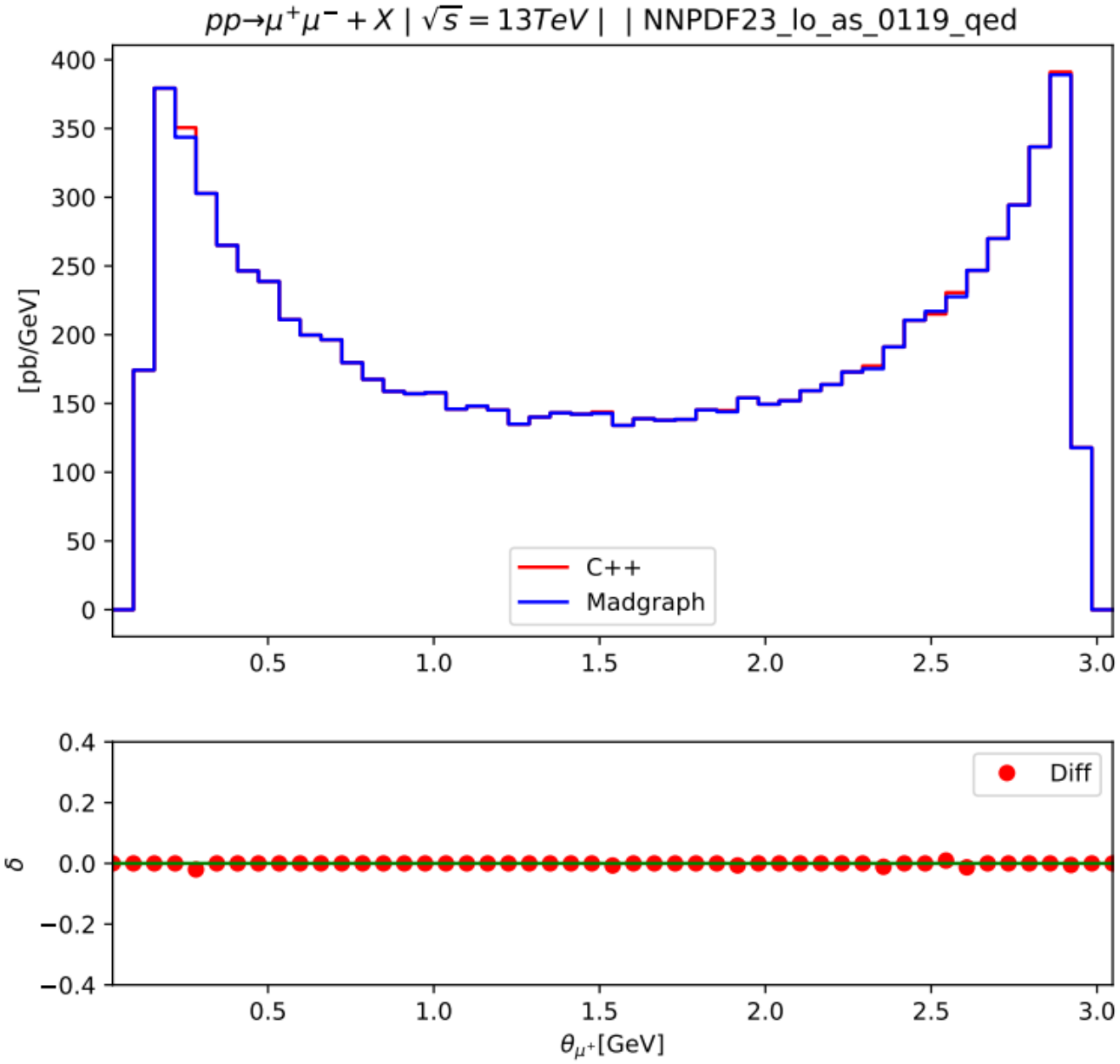

Figure 3.10: Cross section distribution by θ of μ^- of C++ code and Madgraph calculations. The subtiles figure is the different between two results.

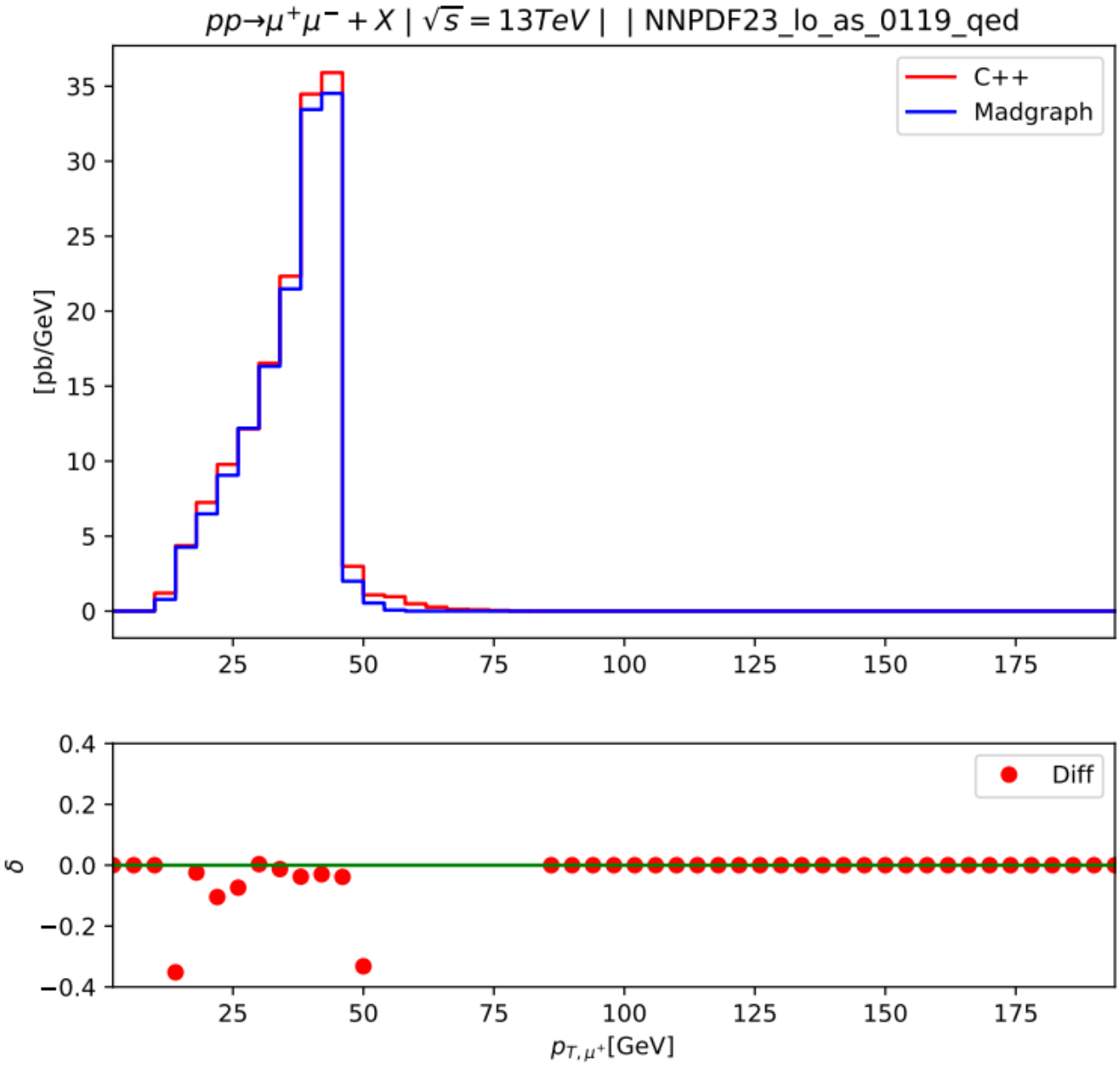

Figure 3.11: Cross section distribution by tranvese momentum of μ^+ of C++ code and Madgraph calculations. The subtiles figure is the different between two results.

We can see that the two distributions by transverse momentum of μ^+ and μ^- are similar, because the transverse momentum of initial quarks are neglected.

Chapter 4

Process $pp \longrightarrow e^+\nu_e\mu^+\mu^- + X$

In this section, we consider the process

$$pp \longrightarrow e^+\nu_e\mu^+\mu^- + X. \tag{4.0.1}$$

We will use the same helicity amplitude method to calculate the amplitudes at leading order. The aim is to calculate the cross section and kinematical distributions as for the $2 \longrightarrow 2$ processes presented in the previous section. However, because of a large number of Feynman diagrams and a complicated phase-space structure (see Section 2.1.2), we have not been able to obtain results at the cross section level in a short time frame. We would like to note that all helicity amplitudes have been calculated and cross checked against Madgraph at a random phase space point. This is the main result of this section. The phase space generation has been implemented in a C++ code and has been presented in Section 2.1.2. However, the numerical integration does not work properly and the results cannot be compared with Madgraph yet. We are working on this and hopefully it will be fixed in the near future.

4.1 Helicity amplitudes

In this collision, we only consider these process:

$$u + \bar{d} \longrightarrow e^+ + \nu_e + \mu^+ + \mu^-, \tag{4.1.2}$$
$$c + \bar{s} \longrightarrow e^+ + \nu_e + \mu^+ + \mu^-. \tag{4.1.3}$$

We have 10 diagrams in total to calculate these processes.

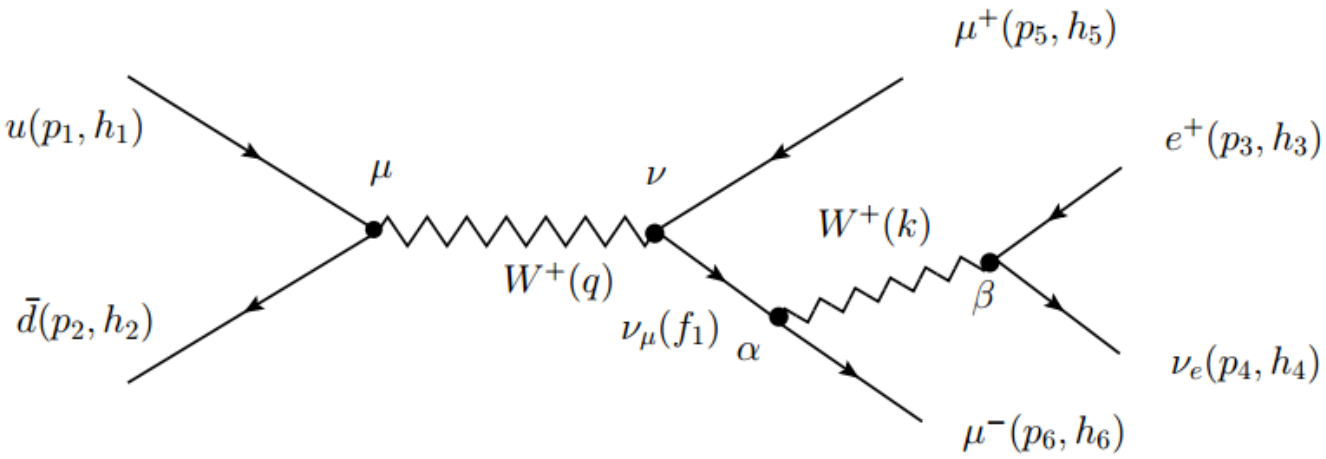

Figure 4.1: (Diagram 1) Only the W^+-boson appears.

In diagram 1, we have:

$$q = p_1 + p_2, \tag{4.1.4}$$
$$k = p_3 + p_4, \tag{4.1.5}$$
$$f_1 = p_3 + p_4 + p_6, \tag{4.1.6}$$
$$\Longrightarrow \not{f}_1 = \not{p}_3 + \not{p}_4 + \not{p}_6, \tag{4.1.7}$$

$$\begin{aligned}
\mathcal{M}_1 &= \Big[\bar{v}(p_2, h_2)\lambda^{\mu}_{W^+u\bar{d}}u(p_1, h_1)\Big] \times D^{W^+}_{\mu\nu}(q) \\
&\times \Big[\bar{u}(p_6, h_6)\lambda^{\alpha}_{W^+\mu\nu_\mu}D_F(f_1)\lambda^{\nu}_{W^+\mu^+\nu_\mu}v(p_5, h_5)\Big] \\
&\times D^{W^+}_{\alpha\beta} \times \Big[\bar{u}(p_4, h_4)\lambda^{\beta}_{W^+e^+\nu_e}v(p_3, h_3)\Big] \\
&= \Big[\bar{v}(p_2, h_2)ie\gamma^{\mu}\frac{1}{\sqrt{2}s_W}P_L u(p_1, h_1)\Big] \times \frac{-i}{q^2 - m_W^2 + iM_W\Gamma_W}\Big[g_{\mu\nu} - (1 - \xi_W)\frac{q_\mu q_\nu}{q^2 - \xi_W M_W^2}\Big] \\
&\times \Big[\bar{u}(p_6, h_6)ie\gamma^{\alpha}\frac{1}{\sqrt{2}s_W}P_L\frac{\not{f}_1}{f_1^2}ibe\gamma^{\nu}\frac{1}{\sqrt{2}s_W}P_L v(p_5, h_5)\Big] \\
&\times \frac{-i}{k^2 - m_W^2 + iM_W\Gamma_W}\Big[g_{\alpha\beta} - (1 - \xi_Z)\frac{k_\alpha k_{beta}}{k^2 - \xi_Z M_Z^2} \times \Big[\bar{u}(p_4, h_4)ie\gamma^{\beta}\frac{1}{\sqrt{2}s_W}P_L v(p_3, h_3)\Big].
\end{aligned} \tag{4.1.8}$$

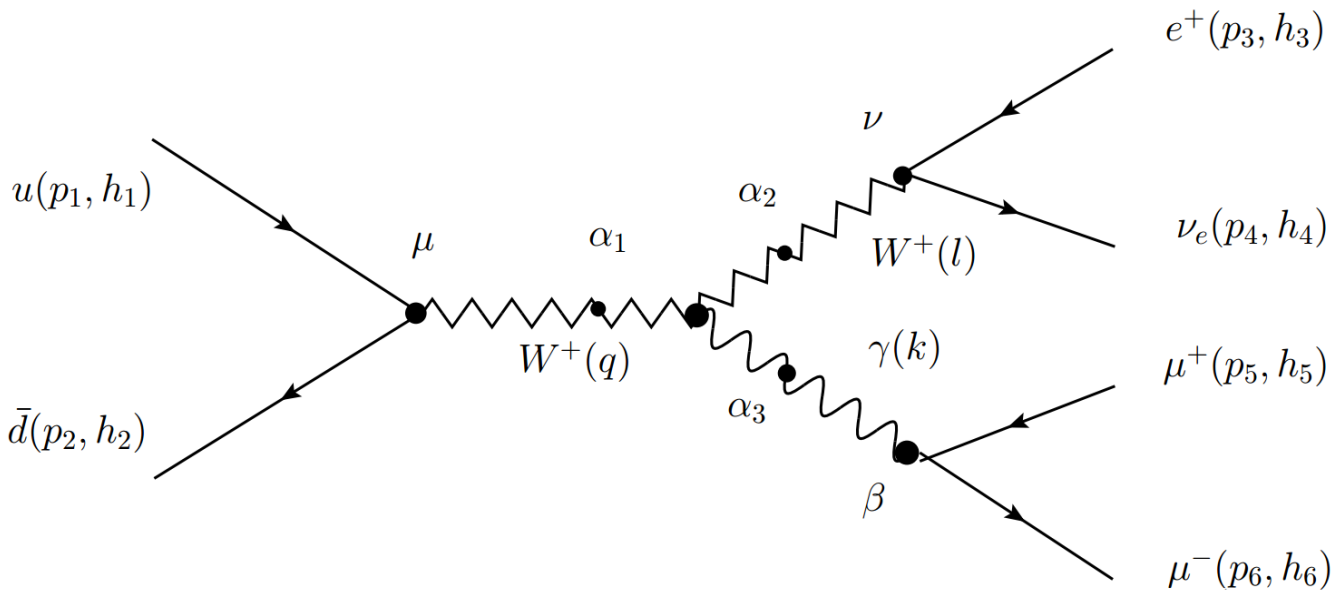

Figure 4.2: (Diagram 2) Photon radiated from W^+.

In diagram 2, we have:

$$q = p_1 + p_2, \tag{4.1.9}$$
$$l = p_3 + p_4, \tag{4.1.10}$$
$$k = p_5 + p_6, \tag{4.1.11}$$

$$\begin{aligned}
\mathcal{M}_2 &= \Big[\bar{v}(p_2, h_2)\lambda^{\mu}_{W^+u\bar{d}}u(p_1, h_1)\Big] \times D^{W^+}_{\mu\alpha_1}(q) \times \Big[\bar{u}(p_3, h_3)\lambda^{\nu}_{W^+e^+\nu_e}v(p_4, h_4)\Big] \times D^{W^+}_{\alpha_2\nu}(l) \\
&\times D^{A}_{\alpha_3\beta}(k) \times \Big[\bar{u}(p_6, h_6)\lambda^{\beta}_{A\mu^+\mu^-}v(p_5, h_5)\Big] \times \lambda^{W^+AW^+}_{\alpha_1\alpha_2\alpha_3} \\
&= \Big[\bar{v}(p_2, h_2)ie\gamma^{\mu}\frac{1}{\sqrt{2}s_W}P_L u(p_1, h_1)\Big] \times \frac{-i}{q^2 - m_W^2 + iM_W\Gamma_W}\Big[g_{\mu\alpha_1} - (1 - \xi_W)\frac{q_\mu q_{\alpha_1}}{q^2 - \xi_W M_W^2}\Big] \\
&\times \frac{-i}{k^2}\Big[g_{\alpha_3\beta} - (1 - \xi_A)\frac{k_{\alpha_3}k_\beta}{k^2}\Big] \times \Big[\bar{u}(p_6, h_6)(-i)e(-1)\gamma^{\beta}v(p_5, h_5)\Big] \\
&\times (-i)e\Big[g^{\alpha_1\alpha_2}(-l - q)^{\alpha_3} + g^{\alpha_2\alpha_3}(-k + l)^{\alpha_1} + g^{\alpha_3\alpha_1}(q + k)^{\alpha_2}\Big].
\end{aligned} \tag{4.1.12}$$

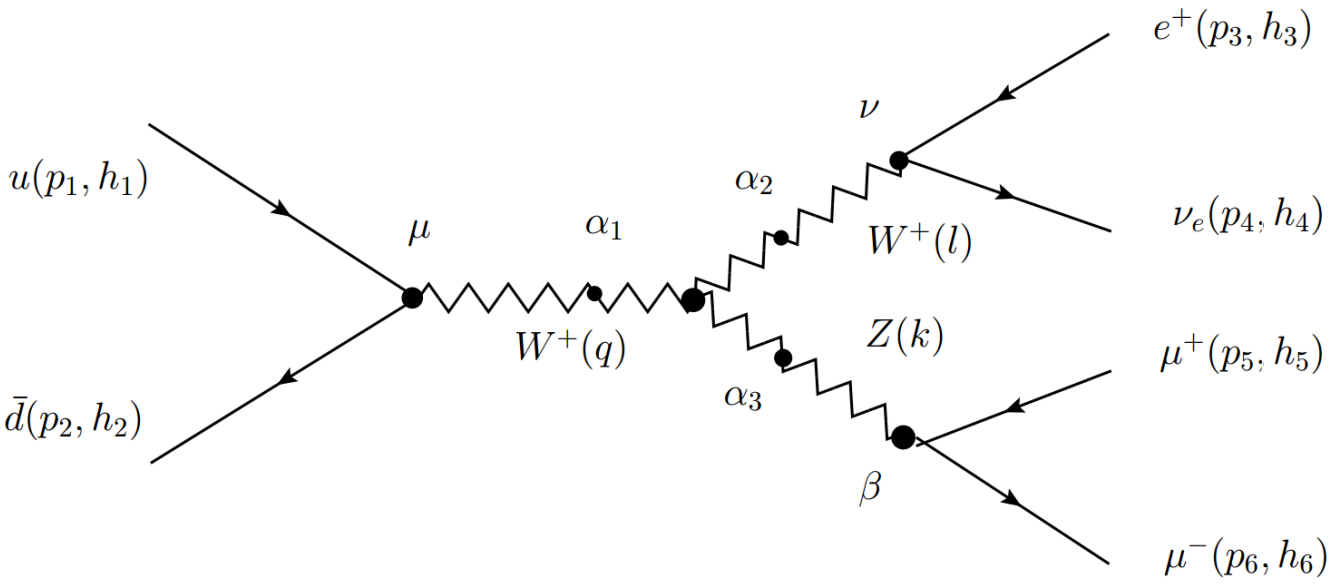

Figure 4.3: (Diagram 3) Z-boson radiated from W^+.

The momenta are equal to Diagram 2.

$$
\begin{aligned}
\mathcal{M}_3 &= \Big[\bar{v}(p_2,h_2)\lambda^{\mu}_{W^+u\bar{d}}u(p_1,h_1)\Big] \times D^{W^+}_{\mu\alpha_1}(q) \times \Big[\bar{u}(p_3,h_3)\lambda^{\nu}_{W^+e^+\nu_e}v(p_4,h_4)\Big] \times D^{W^+}_{\alpha_2\nu}(l) \\
&\times D^{Z}_{\alpha_3\beta}(k) \times \Big[\bar{u}(p_6,h_6)\lambda^{\beta}_{Z\mu^+\mu^-}v(p_5,h_5)\Big] \times \lambda^{W^+ZW^+}_{\alpha_1\alpha_2\alpha_3} \\
&= \Big[\bar{v}(p_2,h_2)ie\gamma^{\mu}\frac{1}{\sqrt{2}s_W}P_L u(p_1,h_1)\Big] \times \frac{-i}{q^2-m_W^2+iM_W\Gamma_W}\Big[g_{\mu\alpha_1}-(1-\xi_W)\frac{q_\mu q_{\alpha_1}}{q^2-\xi_W M_W^2}\Big] \\
&\times \frac{-i}{k^2}\Big[g_{\alpha_3\beta}-(1-\xi_A)\frac{k_{\alpha_3}k_\beta}{k^2}\Big] \times \Big[\bar{u}(p_6,h_6)(-i)e(-1)\gamma^{\beta}v(p_5,h_5)\Big] \\
&\times (-i)e\Big[g^{\alpha_1\alpha_2}(-l-q)^{\alpha_3}+g^{\alpha_2\alpha_3}(-k+l)^{\alpha_1}+g^{\alpha_3\alpha_1}(q+k)^{\alpha_2}\Big].
\end{aligned}
\tag{4.1.13}
$$

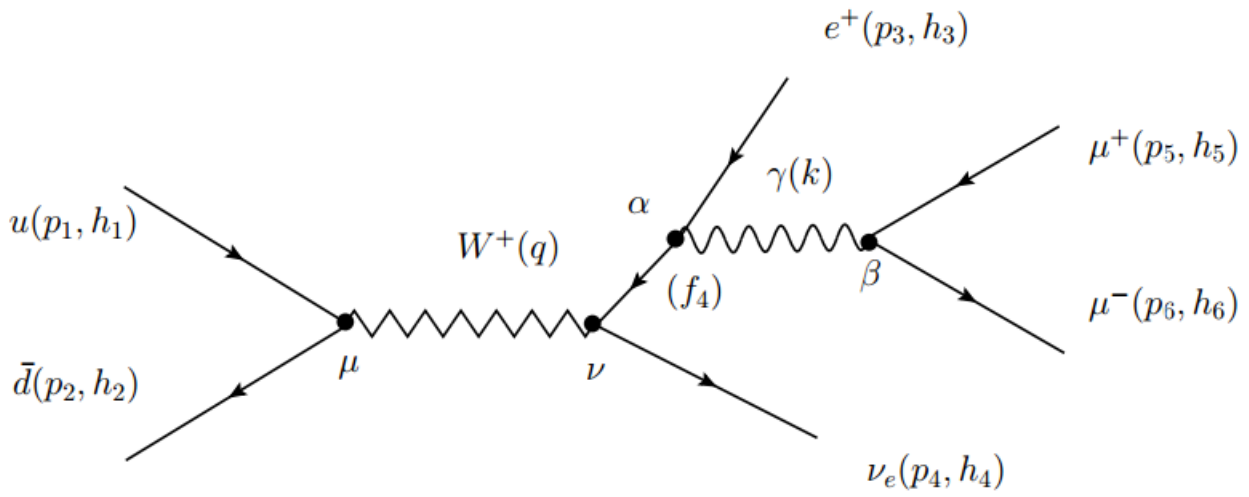

Figure 4.4: (Diagram 4) Photon radiated from e^+.

In diagram 4, we have:

$$q = p_1 + p_2, \tag{4.1.14}$$
$$k = p_5 + p_6, \tag{4.1.15}$$
$$f_4 = p_3 + p_5 + p_6, \tag{4.1.16}$$
$$\Longrightarrow \not{f}_4 = \not{p}_3 + \not{p}_5 + \not{p}_6, \tag{4.1.17}$$

$$\begin{aligned}
\mathcal{M}_4 &= \Big[\bar{v}(p_2, h_2)\lambda^{\mu}_{W^+u\bar{d}}u(p_1, h_1)\Big] \times D^{W^+}_{\mu\nu}(q) \\
&\times \Big[\bar{u}(p_4, h_4)\lambda^{\nu}_{W^+e^+\nu_e}D_F(-f_4)\lambda^{\alpha}_{Ae^+e^-}v(p_3, h_3)\Big] \\
&\times D^{A}_{\alpha\beta}(k) \times \Big[\bar{u}(p_6, h_6)\lambda^{\beta}_{A\mu^+\mu^-}v(p_5, h_5) \\
&= \Big[\bar{v}(p_2, h_2)ie\gamma^{\mu}\frac{1}{\sqrt{2}s_W}P_L u(p_1, h_1)\Big] \times \frac{-i}{q^2 - M_W^2 + iM_W\Gamma_W}\Big[g_{\mu\nu} - (1-\xi_W)\frac{q_\mu q_\nu}{q^2 - \xi_W M_W^2}\Big] \\
&\times \Big[\bar{u}(p_4, h_4)ie\gamma^{\nu}\frac{1}{\sqrt{2}s_W}P_L\frac{-\not{f}_4}{f_f^2}[-ie(-1)\gamma^{\alpha}]v(p_5, h_5)\Big] \\
&\times \frac{-i}{k^2}\Big[g_{\alpha\beta} - (1-\xi_A)\frac{k_\alpha k_\beta}{k^2}\Big] \times \Big[\bar{u}(p_6, h_6)[ie\gamma^{\beta}\frac{I_3^{\mu}(1-\gamma^5) - 2s_W^2 Q_{\mu}}{2s_W c_W}v(p_5, h_5)].
\end{aligned} \tag{4.1.18}$$

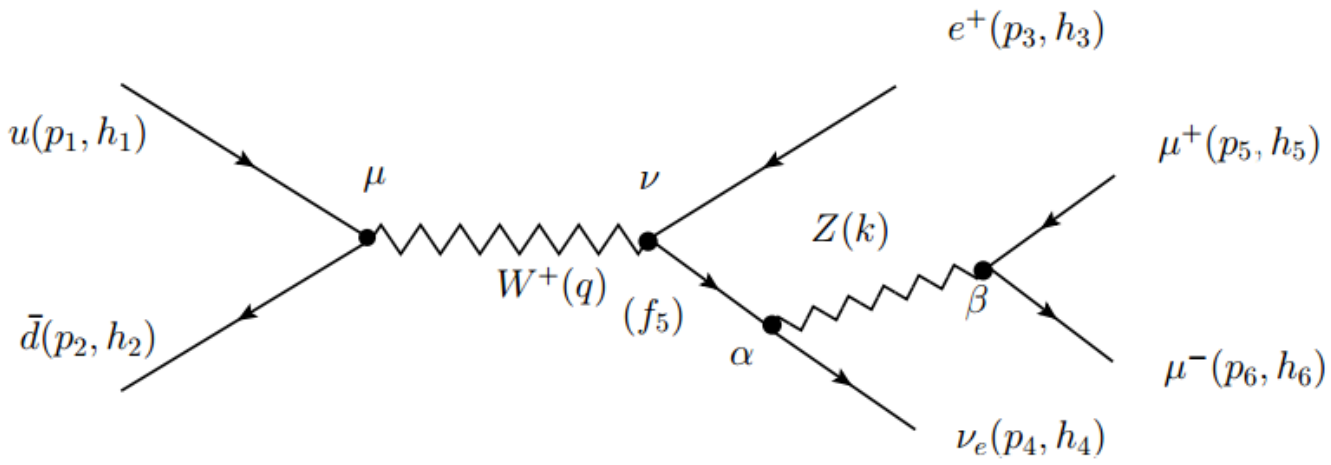

Figure 4.5: (Diagram 5) Z-boson radiated from electron neutrino.

In diagram 5. we have:

$$q = p_1 + p_2, \tag{4.1.19}$$
$$k = p_5 + p_6, \tag{4.1.20}$$
$$f_5 = p_4 + p_5 + p_6, \tag{4.1.21}$$
$$\Longrightarrow \not{f}_5 = \not{p}_4 + \not{p}_5 + \not{p}_6, \tag{4.1.22}$$

$$\begin{aligned}
\mathcal{M}_5 &= \Big[\bar{v}(p_2, h_2)\lambda^{\mu}_{W^+u\bar{d}}u(p_1, h_1)\Big] \times D^{W^+}_{\mu\nu}(q) \\
&\times \Big[\bar{u}(p_4, h_4)\lambda^{\alpha}_{Z\nu\bar{\nu}}D_F(f_5)\lambda^{\nu}_{W^+e^+\nu_e}v(p_3, h_3)\Big] \\
&\times D^{Z}_{\alpha\beta}(k) \times \Big[\bar{u}(p_6, h_6)\lambda^{\beta}_{Z\mu^+\mu^-}v(p_5, h_5)\Big] \\
&= \Big[\bar{v}(p_2, h_2)ie\gamma^{\mu}\frac{1}{\sqrt{2}s_W}P_L u(p_1, h_1)\Big] \times \frac{-i}{q^2 - M_W^2 + iM_W\Gamma_W}\Big[g_{\mu\nu} - (1-\xi_W)\frac{q_\mu q_\nu}{q^2 - \xi_W M_W^2}\Big] \\
&\times \Big[\bar{u}(p_4, h_4)ie\gamma^{\alpha}\frac{I_3^{\nu_e}(1-\gamma^5) - 2s_W^2 Q_{\nu_e}}{2s_W c_W}D_F(f_5)ie\gamma^{\nu}\frac{1}{\sqrt{2}s_W}P_L v(p_3, h_3)\Big] \\
&\times \frac{-i}{k^2 - M_Z^2 + iM_Z\Gamma_Z}\Big[g_{\alpha\beta} - (1-\xi_Z)\frac{k_\alpha k_\beta}{k^2 - \xi_Z M_Z^2}\Big] \times \Big[\bar{u}(p_6, h_6)ie\gamma^{\beta}\frac{I_3^{\mu}(1-\gamma^5) - 2s_W^2 Q_{\mu}}{2s_W c_W}v(p_5, h_5)\Big].
\end{aligned} \tag{4.1.23}$$

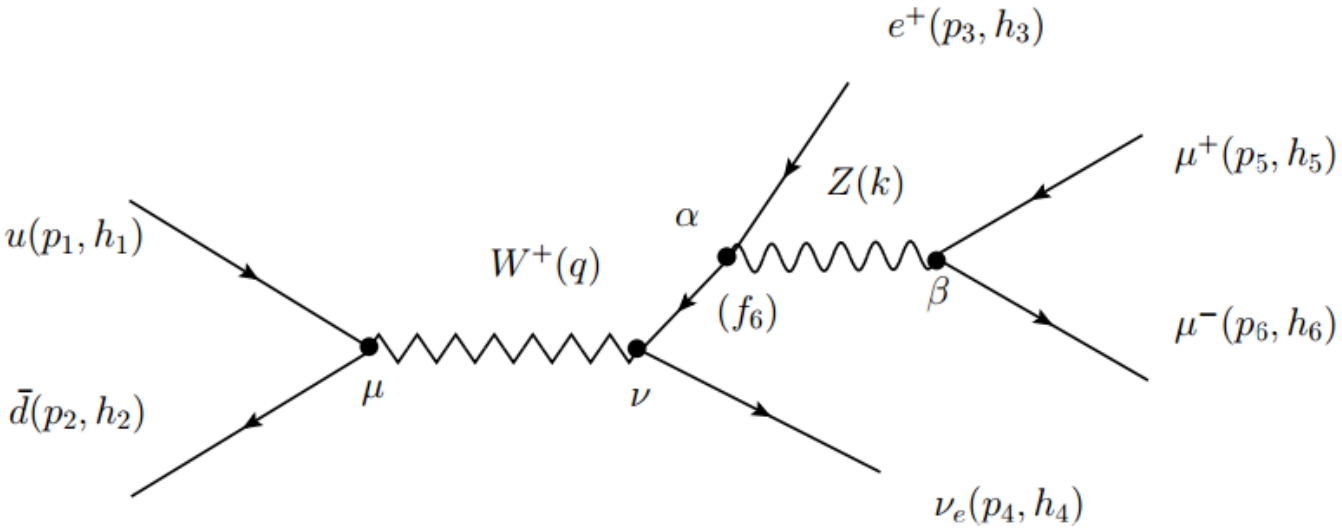

Figure 4.6: (Diagram 6) Z-boson radiated from e^+.

In diagram 6, we have:

$$q = p_1 + p_2, \tag{4.1.24}$$
$$k = p_5 + p_6, \tag{4.1.25}$$
$$f_6 = p_3 + p_5 + p_6, \tag{4.1.26}$$
$$\Longrightarrow \not{f}_6 = \not{p}_3 + \not{p}_5 + \not{p}_6, \tag{4.1.27}$$

$$\begin{aligned}
\mathcal{M}_6 &= \Big[\bar{v}(p_2,h_2)\lambda^{\mu}_{W^+u\bar{d}}u(p_1,h_1)\Big] \times D^{W^+}_{\mu\nu}(q) \\
&\times \Big[\bar{u}(p_4,h_4)\lambda^{\nu}_{W^+e^+\nu_e}D_F(-f_6)\lambda^{\alpha}_{Zee}v(p_3,h_3)\Big] \\
&\times D^{Z}_{\alpha\beta}(k) \times \Big[\bar{u}(p_6,h_6)\lambda^{\beta}_{Z\mu^+\mu^-}v(p_5,h_5)\Big] \\
&= \Big[\bar{v}(p_2,h_2)ie\gamma^{\mu}\frac{1}{\sqrt{2}s_W}P_L u(p_1,h_1)\Big] \times \frac{-i}{q^2 - M_W^2 + iM_W\Gamma_W}\Big[g_{\mu\nu} - (1-\xi_W)\frac{q_\mu q_\nu}{q^2 - \xi_W M_W^2}\Big] \\
&\times \Big[\bar{u}(p_4,h_4)ie\gamma^{\nu}\frac{1}{\sqrt{2}s_W}P_L\frac{-\not{f}_6}{f_6^2}ie\gamma^{\alpha}\frac{I_3^e(1-\gamma^5) - 2s_W^2Q_e}{2s_Wc_W}v(p_3,h_3)\Big] \\
&\times \frac{-i}{k^2 - M_Z^2 + iM_Z\Gamma_Z}\Big[g_{\alpha\beta} - (1-\xi_Z)\frac{k_\alpha k_\beta}{k^2 - \xi_Z M_Z^2}\Big] \times \Big[\bar{u}(p_6,h_6)ie\gamma^{\beta}\frac{I_3^{\mu}(1-\gamma^5) - 2s_W^2Q_{\mu}}{2s_Wc_W}v(p_5,h_5)\Big].
\end{aligned} \tag{4.1.28}$$

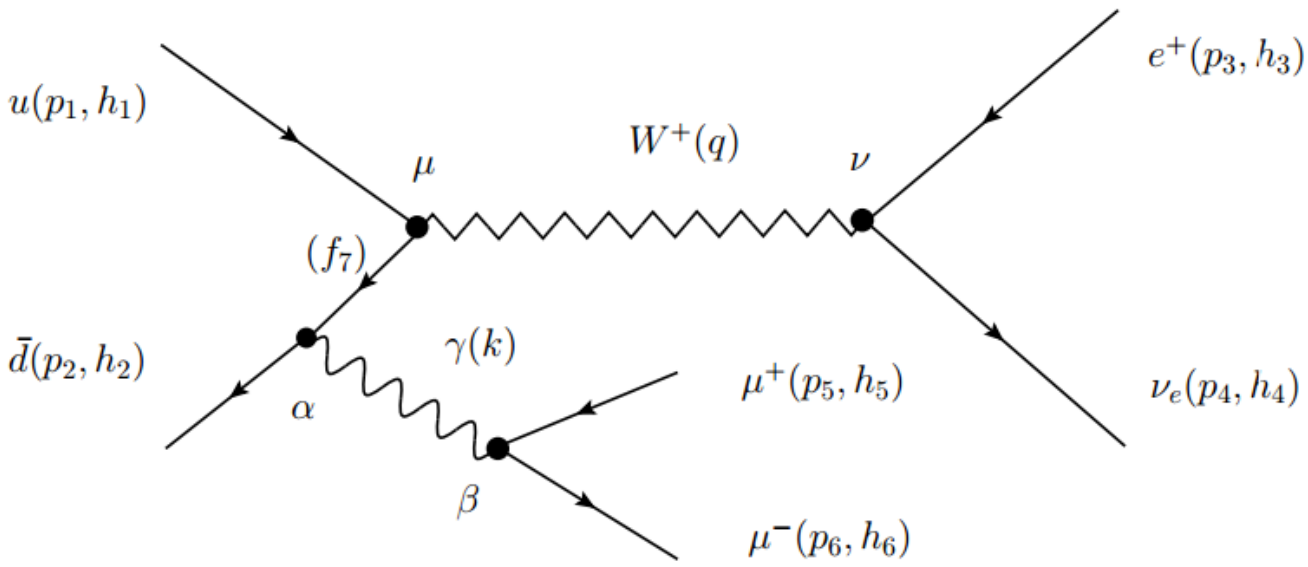

Figure 4.7: (Diagram 7) Photon radiated from $\bar{d}$.

In diagram 7, we have:

$$q = p_3 + p_4, \tag{4.1.29}$$
$$k = p_5 + p_6, \tag{4.1.30}$$
$$f_7 = p_2 - p_5 - p_6, \tag{4.1.31}$$
$$\implies \not{f}_7 = \not{p}_2 - \not{p}_5 - \not{p}_6, \tag{4.1.32}$$

$$\begin{aligned}
\mathcal{M}_7 &= \Big[\bar{v}(p_2, h_2)\lambda^{\alpha}_{Ad\bar{d}} D_F(-f_7)\lambda^{\mu}_{W^+u\bar{d}} u(p_1, h_1)\Big] \\
&\times D^{W^+}_{\mu\nu}(q) \times \Big[\bar{u}(p_4, h_4)\lambda^{\nu}_{W^+e^+\nu_e} v(p_3, h_3)\Big] \\
&\times D^{\gamma}_{\alpha\beta}(k) \times \Big[\bar{u}(p_6, h_6)\lambda^{\beta}_{A\mu^+\mu^-} v(p_5, h_5)\Big] \\
&= \Big[\bar{v}(p_2, h_2)(-i)eQ_d\gamma^{\alpha}\frac{-\not{f}_7}{f_7^2} ie\gamma^{\mu}\frac{1}{\sqrt{2}s_W}P_L u(p_1, h_1)\Big] \\
&\times \frac{-i}{q^2 - M_W^2 + iM_W\Gamma_W}\Big[g_{\mu\nu} - (1-\xi_W)\frac{q_\mu q_\nu}{q^2 - \xi_W M_W^2}\Big] \times \Big[\bar{u}(p_4, h_4) ie\gamma^{\nu}\frac{1}{\sqrt{2}s_W}P_L v(p_3, h_3)\Big] \\
&\times \frac{-i}{k^2}\Big[g_{\alpha\beta} - (1-\xi_A)\frac{k_\alpha k_\beta}{k^2}\Big] \times \Big[\bar{u}(p_6, h_6)(-i)eQ_\mu v(p_5, h_5)\Big].
\end{aligned} \tag{4.1.33}$$

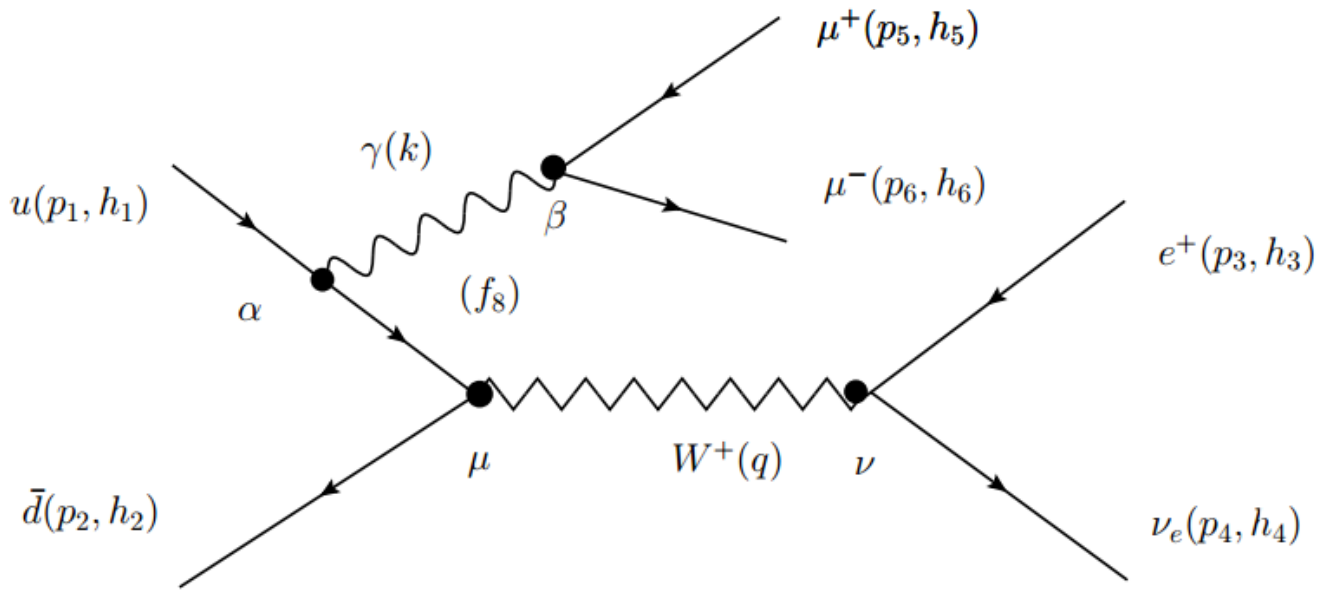

Figure 4.8: (Diagram 8) Photon radiated from u.

In diagram 8, we have:

$$q = p_3 + p_4, \tag{4.1.34}$$
$$k = p_5 + p_6, \tag{4.1.35}$$
$$f_8 = p_1 - p_5 - p_6, \tag{4.1.36}$$
$$\Longrightarrow \not{f}_8 = \not{p}_1 - \not{p}_5 - \not{p}_6, \tag{4.1.37}$$

$$\begin{aligned}
\mathcal{M}_8 = &\Big[\bar{v}(p_2, h_2)\lambda^{\mu}_{W^+u\bar{d}} D_F(f_8)\lambda^{\alpha}_{Au\bar{u}} u(p_1, h_1)\\
&\times D^{W^+}_{\mu\nu}(q) \times \Big[\bar{u}(p_4, h_4)\lambda^{\nu}_{W^+e^+\nu_e} v(p_3, h_3)\Big]\\
&\times D^{\gamma}_{\alpha\beta}(k) \times \Big[\bar{u}(p_6, h_6)\lambda^{\beta}_{A\mu^+\mu^-} v(p_5, h_5\Big]\\
&= \Big[\bar{v}(p_2, h_2) ie\gamma^{\mu} \frac{1}{\sqrt{2}s_W} P_L \frac{\not{f}_8}{f_8^2} (-i) eQ_u \gamma^{\alpha} u(p_1, h_1)\Big]\\
&\times \frac{-i}{q^2 - M_W^2 + iM_W\Gamma_W}\Big[g_{\mu\nu} - (1-\xi_W)\frac{q_\mu q_\nu}{q^2 - \xi_W M_W^2}\Big] \times \Big[\bar{u}(p_4, h_4) ie\gamma^{\nu} \frac{1}{\sqrt{2}s_W} P_L v(p_3, h_3)\Big]\\
&\times \frac{-i}{k^2}\Big[g_{\alpha\beta} - (1-\xi_A)\frac{k_\alpha k_\beta}{k^2}\Big] \times \Big[\bar{u}(p_6, h_6)(-i)eQ_\mu v(p_5, h_5)\Big].
\end{aligned} \tag{4.1.38}$$

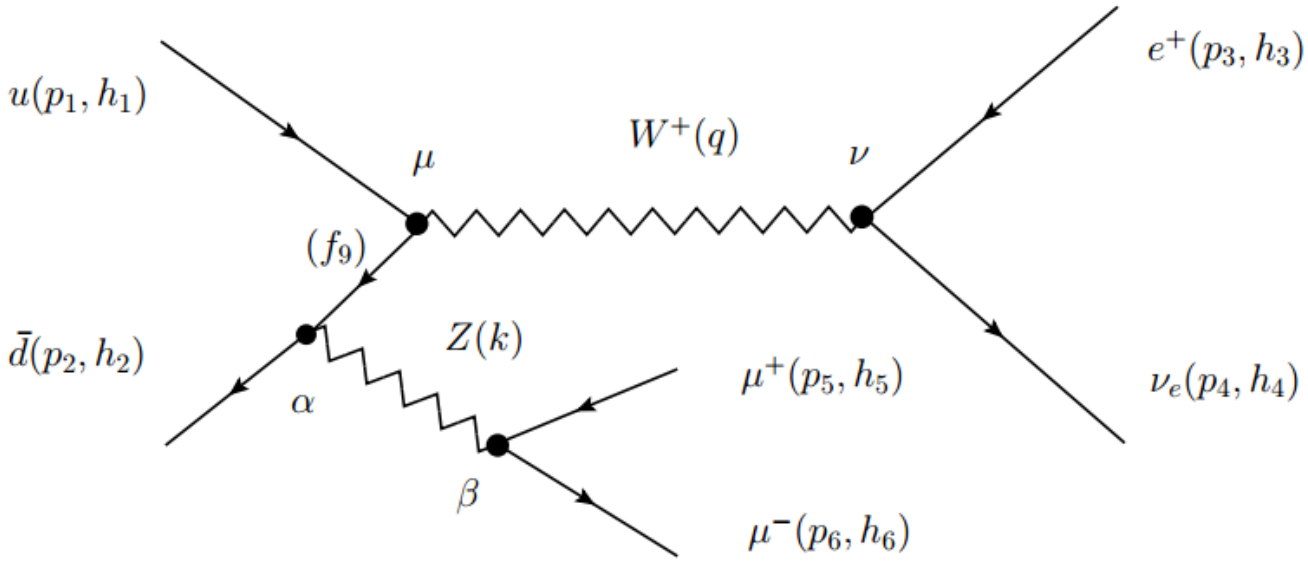

Figure 4.9: (Diagram 9) Z-boson radiated from $\bar{d}$.

In diagram 9, we have:

$$q = p_3 + p_4, \tag{4.1.39}$$
$$k = p_5 + p_6, \tag{4.1.40}$$
$$f_9 = p_2 - p_5 - p_6, \tag{4.1.41}$$
$$\Longrightarrow \not{f}_9 = \not{p}_2 - \not{p}_5 - \not{p}_6, \tag{4.1.42}$$

$$\begin{aligned}
\mathcal{M}_9 &= \left[\bar{v}(p_2, h_2)\lambda^{\alpha}_{Zd\bar{d}} D_F(-f_9)\lambda^{\mu}_{W^+u\bar{d}} u(p_1, h_1)\right] \\
&\times D^{W^+}_{\mu\nu}(q) \times \left[\bar{u}(p_4, h_4)\lambda^{\nu}_{W^+e^+\nu_e} v(p_3, h_3)\right] \\
&\times D^{Z}_{\alpha\beta}(k) \times \left[\bar{u}(p_6, h_6)\lambda^{\beta}_{Z\mu^+\mu^-} v(p_5, h_5\right] \\
&= \left[\bar{v}(p_2, h_2) ie\gamma^{\alpha} \frac{I_3^d(1-\gamma^5) - 2s_W^2 Q_d}{2s_W c_W} \frac{-\not{f}_9}{f_9^2} ie\gamma^{\mu} \frac{1}{\sqrt{2}s_W} P_L u(p_1, h_1)\right] \\
&\times \frac{-i}{q^2 - M_W^2 + iM_W\Gamma_W}\left[g_{\mu\nu} - (1-\xi_W)\frac{q_\mu q_\nu}{q^2 - \xi_W M_W^2}\right] \times \left[\bar{u}(p_4, h_4) ie\gamma^{\nu} \frac{1}{\sqrt{2}s_W} P_L v(p_3, h_3)\right] \\
&\times \frac{-i}{k^2 - M_Z^2 + iM_Z\Gamma_Z}\left[g_{\alpha\beta} - (1-\xi_Z)\frac{k_\alpha k_\beta}{k^2 - \xi_Z M_Z^2}\right] \times \left[\bar{u}(p_6, h_6) ie\gamma^{\beta} \frac{I_3^{\mu}(1-\gamma^5) - 2s_W^2 Q_{\mu}}{2s_W c_W} v(p_5, h_5)\right].
\end{aligned} \tag{4.1.43}$$

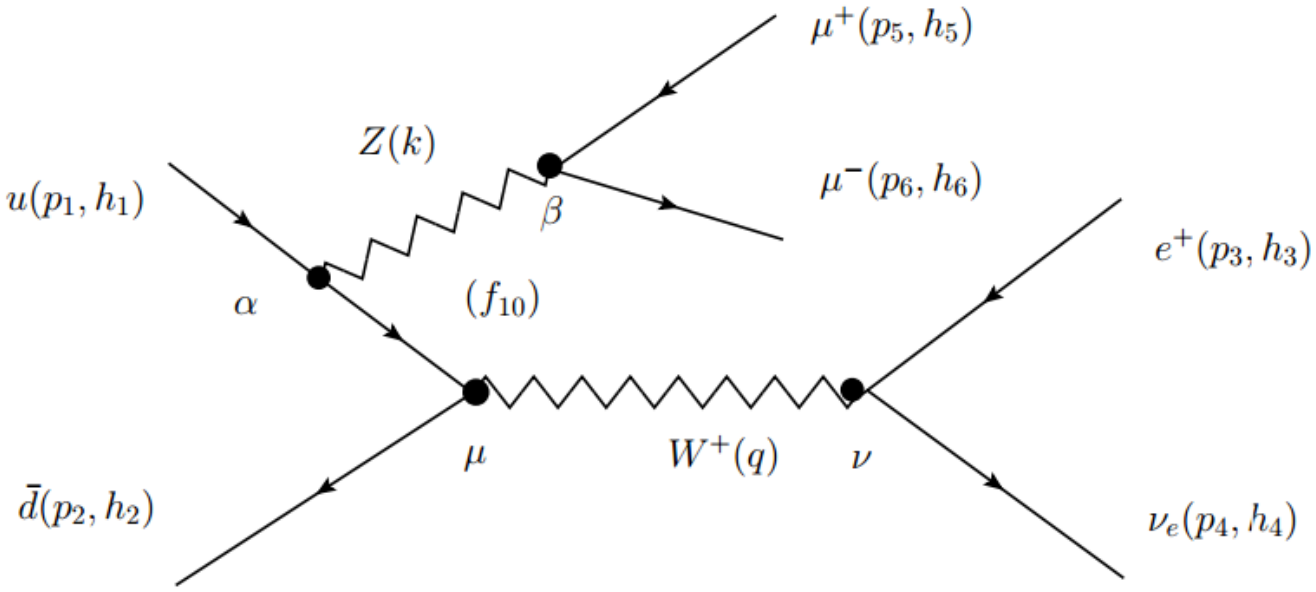

Figure 4.10: (Diagram 10) Z-boson radiated from u.

In diagram 10, we have:

$$q = p_3 + p_4, \tag{4.1.44}$$
$$k = p_5 + p_6, \tag{4.1.45}$$
$$f_{10} = p_1 - p_5 - p_6, \tag{4.1.46}$$
$$\implies \not{f}_{10} = \not{p}_1 - \not{p}_5 - \not{p}_6, \tag{4.1.47}$$

$$\begin{aligned}
\mathcal{M}_{10} = &\Big[\bar{v}(p_2, h_2)\lambda^{\mu}_{W^+u\bar{d}} D_F(f_{10})\lambda^{\alpha}_{Zu\bar{u}} u(p_1, h_1) \\
&\times D^{W^+}_{\mu\nu}(q) \times \Big[\bar{u}(p_4, h_4)\lambda^{\nu}_{W^+e^+\nu_e} v(p_3, h_3)\Big] \\
&\times D^{Z}_{\alpha\beta}(k) \times \Big[\bar{u}(p_6, h_6)\lambda^{\beta}_{Z\mu^+\mu^-} v(p_5, h_5)\Big] \\
&= \Big[\bar{v}(p_2, h_2) ie\gamma^{\mu} \frac{1}{\sqrt{2}s_W} P_L \frac{\not{f}_{10}}{f_{10}^2} ie\gamma^{\alpha} \frac{I_3^u(1-\gamma^5) - 2s_W^2 Q_u}{2s_W c_W} u(p_1, h_1)\Big] \\
&\times \frac{-i}{q^2 - M_W^2 + iM_W\Gamma_W}\Big[g_{\mu\nu} - (1-\xi_W)\frac{q_\mu q_\nu}{q^2 - \xi_W M_W^2}\Big] \times \Big[\bar{u}(p_4, h_4) ie\gamma^{\nu} \frac{1}{\sqrt{2}s_W} P_L v(p_3, h_3)\Big] \\
&\times \frac{-i}{k^2 - M_Z^2 + iM_Z\Gamma_Z}\Big[g_{\alpha\beta} - (1-\xi_Z)\frac{k_\alpha k_\beta}{k^2 - \xi_Z M_Z^2}\Big] \times \Big[\bar{u}(p_6, h_6) ie\gamma^{\beta} \frac{I_3^{\mu}(1-\gamma^5) - 2s_W^2 Q_{\mu}}{2s_W c_W} v(p_5, h_5)\Big].
\end{aligned} \tag{4.1.48}$$

4.2 Results at one phase space point

In experiments, we don't know the helicity of the incoming particles. We also don't know the color of the incoming quarks. Because of these reasons, we have to average over the helicities and colors over the incoming quarks. We than have

$$\begin{aligned}|\bar{\mathcal{M}}|^2 &= \frac{1}{2}\times\frac{1}{2}\times\frac{1}{3}\times\frac{1}{3}\times\sum_{i,j=1}^{3}\delta_{ij}\delta_{ij}\times\sum_{h_1,h_3,h_5=-1}^{1}\mathcal{M}^{\dagger}\mathcal{M}\\ &= \frac{1}{12}\sum_{h_1,h_3,h_5}^{1}\mathcal{M}^{\dagger}\mathcal{M},\end{aligned} \tag{4.2.49}$$

which

$$(h_1,h_3,h_5) = \pm 1, \tag{4.2.50}$$

and the helicity condition for each vertex:

$$\begin{cases} h_2 &= -h_1,\\ h_4 &= -h_3,\\ h_6 &= -h_5. \end{cases} \tag{4.2.51}$$

Using the Monte Carlo method, we can generate any phase space point. In the following, we provide the results for the squared amplitudes at the following phase space point given in the GeV unit

$$u(p_1)\colon \begin{cases} E^{u} &= 5461.2201615056129\\ p_x^{u} &= 0.0\\ p_y^{u} &= 0.0\\ p_z^{u} &= 5461.2201615056129 \end{cases} \tag{4.2.52}$$

$$\bar{d}(p_2)\colon \begin{cases} E^{\bar{d}} &= 0.29329208900798337\\ p_x^{\bar{d}} &= 0.0\\ p_y^{\bar{d}} &= 0.0\\ p_z^{\bar{d}} &= -0.29329208900798337 \end{cases} \tag{4.2.53}$$

$$e^{+}(p_3)\colon \begin{cases} E^{e^+} &= 92.789966932159857\\ p_x^{e^+} &= 3.5926921940028631\\ p_y^{e^+} &= 9.5831433076758099\\ p_z^{e^+} &= 92.223824960880648 \end{cases} \tag{4.2.54}$$

$$\nu_e(p_4)\colon \begin{cases} E^{\nu_e} &= 5120.8512713042473\\ p_x^{\nu_e} &= -3.2928507598614218\\ p_y^{\nu_e} &= -10.537695392820094\\ p_z^{\nu_e} &= 5120.8393703501388 \end{cases} \tag{4.2.55}$$

$$\mu^+(p_5): \begin{cases} E^{\mu^+} & = 143.54763095164728 \\ p^{\mu^+} & = -0.051940546572615778 \\ p^{\mu^+} & = -0.32652450618650886 \\ p^{\mu^+} & = 143.54725018528501 \end{cases} \tag{4.2.56}$$

$$\mu^-(p_6): \begin{cases} E^{\mu^-} & = 104.324584406575 \\ p_x^{\mu^-} & = -0.24790088756886308 \\ p_y^{\mu^-} & = 1.2810765913309128 \\ p_z^{\mu^-} & = 104.3164239203093 \end{cases} \tag{4.2.57}$$

From this phase space point, using our C++ code, we can compare with Madgraph. The results has provied in Table 4.1.

Diagram	C++ code	Madgraph
Diagram 1: $\lvert\mathcal{M}_1\rvert^2$	1.81793816613e-10	1.81793816649e-10
Diagram 2: $\lvert\mathcal{M}_2\rvert^2$	0.00905783314712	0.00905783314638
Diagram 3: $\lvert\mathcal{M}_3\rvert^2$	1.73049375779e-09	1.73049375759e-09
Diagram 4: $\lvert\mathcal{M}_4\rvert^2$	0.0288615815437	0.0288615815705
Diagram 5: $\lvert\mathcal{M}_5\rvert^2$	1.70721007491e-11	1.70721007492e-11
Diagram 6: $\lvert\mathcal{M}_6\rvert^2$	7.04347938134e-10	7.04347938151e-10
Diagram 7: $\lvert\mathcal{M}_7\rvert^2$	0.000484856100443	0.000484856100374
Diagram 8: $\lvert\mathcal{M}_8\rvert^2$	0.000316121834019	0.000316121834025
Diagram 9: $\lvert\mathcal{M}_9\rvert^2$	2.50977685423e-10	2.50977685417e-10
Diagram 10: $\lvert\mathcal{M}_{10}\rvert^2$	2.84419700355e-11	2.84419700389e-11
All diagrams	0.00689708013746	0.00689708013886

Table 4.1: Total Feynman amplitudes for each and all diagrams.

These results agreed with Madgraph, which is needed for our calculation of the total cross section and kinematical distributions in the future.

Conclusion and outlook

Conclusion

Based on what we have done so far in this thesis, we can draw some important conclusion for the calculation techniques in proton-proton collision:

- The helicity amplitude method, which we used to calculate the Feynman amplitudes in Chapter 3 and Chapter 4, is very powerful compared to the squared amplitude method.
- The Monte Carlo method is used to calculate cross sections. Moreover, it can generate any kinematical distributions. We have successfully used this method to calculate polar angle and transverse momentum distributions for $e^+\nu_e$ and $\mu^+\mu^-$ production processes at the LHC. Our results agree well with Madgraph. To reduce integration errors, we have changed the integration variables to smooth out the Breit-Wigner propagator of the W and Z bosons. This makes the integration more efficient.
- When calculating proton-proton cross sections, we must include parton distribution functions. They are provided by the LHAPDF library. The order of the PDF set should match with our calculation order to give a consistent result.
- For the $e^+\nu_e\mu^+\mu^-$ production, the 3-gauge boson coupling diagrams must be included. All helicity amplitudes for this process has been calculated and cross checked against Madgraph.

I would like to note that I have written a C++ code to implement the Monte Carlo integration method. The helicity amplitudes are calculated using a self-made FORM code. The input of this code is the amplitude expressions as given by the Feynman rules without any simplification. The output is written in terms of simple functions, which are scalar products of two spinors, ready for numerical calculations. Dirac equations and on-shell condition for external particles are used in the process. Finally, Feynman diagrams are made using JaxoDraw and plots are produced using Python.

Outlook

As explained in Chapter 4, the cross section and kinematical distributions for the process $pp \longrightarrow e^+\nu_e\mu^+\mu^- + X$ ill be calculated in the future. From there, we will upgrade our result to compare with experimental results provided in Ref. [12] for polarization observables. We expect that, for these special observables, the LO results are not so far from the full results.

Appendix A

Lorentz transformations

Consider a proton-proton scattering into leptons, we have three frame to work with:

- The propagator (vector boson frame).
- The Partonic center of mass frame.
- The laboratory frame.

Kinematical distributions are measured in the laboratory frame, but our calculation is often do in the Vector boson frames and the Partonic Center of mass frame (momentum). To match our calculation with the experiment result, we must have momentum transformation like these step:

Momentum: Vector boson frame $\longrightarrow$ PCMs $\longrightarrow$ Laboratory frame.

The tranformation from Partonic center of mass frame to laboratory frame is boosting along z-axis. The transformation from Vector boson frames to PCMs is boosting along the direction with the momentum of that vector boson (in PCMs).

The general Lorentz transformations (Ref. [13]) are:

$$\mathbf{p}' = \mathbf{p} + \gamma\mathbf{v}\Big(\frac{\gamma\mathbf{v}\cdot\mathbf{p}}{\gamma+1} - E\Big)c^{-2}, \tag{A.0.1}$$

$$E' = \gamma(E - \mathbf{v}\cdot\mathbf{p}), \tag{A.0.2}$$

with the velocity and γ factor of a particle are related to its energy and momentum by the equation:

$$\mathbf{v} = c^2\mathbf{p}/E, \tag{A.0.3}$$
$$\gamma(v) = E/mc^2, \tag{A.0.4}$$
$$\mathbf{v}\gamma(v) = \mathbf{p}/m. \tag{A.0.5}$$

Appendix B

Helicity amplitude method

B.1 Chiral presentation

e using the chiral representation, which have the gamma matrices as:

$$\gamma^0 = \begin{pmatrix} 0 & 0 & 1 & 0 \\ 0 & 0 & 0 & 1 \\ 1 & 0 & 0 & 0 \\ 0 & 1 & 0 & 0 \end{pmatrix} \quad ; \quad \gamma^1 = \begin{pmatrix} 0 & 0 & 0 & 1 \\ 0 & 0 & 1 & 0 \\ 0 & -1 & 0 & 0 \\ -1 & 0 & 0 & 0 \end{pmatrix};$$
$$\gamma^2 = \begin{pmatrix} 0 & 0 & 0 & -i \\ 0 & 0 & i & 0 \\ 0 & i & 0 & 0 \\ -i & 0 & 0 & 0 \end{pmatrix} \quad ; \quad \gamma^3 = \begin{pmatrix} 0 & 0 & 1 & 0 \\ 0 & 0 & 0 & -1 \\ -1 & 0 & 0 & 0 \\ 0 & 1 & 0 & 0 \end{pmatrix}; \tag{B.1.1}$$
$$\gamma^5 = i\gamma^0\gamma^1\gamma^2\gamma^3 = \begin{pmatrix} -1 & 0 & 0 & 0 \\ 0 & -1 & 0 & 0 \\ 0 & 0 & 1 & 0 \\ 0 & 0 & 0 & 1 \end{pmatrix}.$$

The Projection operators:

$$P_L = \frac{1-\gamma^5}{2} = \begin{pmatrix} 1 & 0 & 0 & 0 \\ 0 & 1 & 0 & 0 \\ 0 & 0 & 0 & 0 \\ 0 & 0 & 0 & 0 \end{pmatrix} \quad ; \quad P_R = \frac{1+\gamma^5}{2} = \begin{pmatrix} 0 & 0 & 0 & 0 \\ 0 & 0 & 0 & 0 \\ 0 & 0 & 1 & 0 \\ 0 & 0 & 0 & 1 \end{pmatrix}. \tag{B.1.2}$$

B.2 Weyl and Dirac spinors

The Weyl spinors are:

$$\chi(p,+) = \frac{1}{\sqrt{2|\vec{p}|(|\vec{p}|+p_z)}} \begin{pmatrix} |\vec{p}|+p_z \\ p_x+ip_y \end{pmatrix} \quad ; \quad \chi(p,-) = \frac{1}{\sqrt{2|\vec{p}|(|\vec{p}|+p_z)}} \begin{pmatrix} -p_x+ip_y \\ |\vec{p}|+p_z \end{pmatrix}. \tag{B.2.3}$$

Then the Dirac spinors can be constructed from the Weyl spinors:

$$u(p,\lambda) = \begin{pmatrix} \sqrt{p_0-\lambda|\vec{p}|}\chi(p,\lambda) \\ \sqrt{p_0+\lambda|\vec{p}|}\chi(p,\lambda) \end{pmatrix} \quad ; \quad v(p,\lambda) = \begin{pmatrix} -\lambda\sqrt{p_0+\lambda|\vec{p}|}\chi(p,-\lambda) \\ \lambda\sqrt{p_)-\lambda|\vec{p}|}\chi(p,-\lambda) \end{pmatrix}. \tag{B.2.4}$$

For the massless fermions, they have:

$$p_0 = |\vec{p}|. \tag{B.2.5}$$

Therefore, the massless fermion's spinors are:

$$u(p,+) = \begin{pmatrix} \sqrt{p_0 - |\vec{p}|}\chi(p,+) \\ \sqrt{p_0 + |\vec{p}|}\chi(p,+) \end{pmatrix} = \frac{1}{\sqrt{|\vec{p}| + p_z}} \begin{pmatrix} 0 \\ 0 \\ |\vec{p}| + p_z \\ p_x + ip_y \end{pmatrix}, \tag{B.2.6}$$

$$u(p,-) = \begin{pmatrix} \sqrt{p_0 + |\vec{p}|}\chi(p,-) \\ \sqrt{p_0 - |\vec{p}|}\chi(p,-) \end{pmatrix} = \frac{1}{\sqrt{|\vec{p}| + p_z}} \begin{pmatrix} -p_x + ip_y \\ |\vec{p}| + p_z \\ 0 \\ 0 \end{pmatrix}, \tag{B.2.7}$$

$$v(p,+) = \begin{pmatrix} -\sqrt{p_0 + |\vec{p}|}\chi(p,-) \\ \sqrt{p_0 - |\vec{p}|}\chi(p,-) \end{pmatrix} = \frac{-1}{\sqrt{|\vec{p}| + p_z}} \begin{pmatrix} -p_x + ip_y \\ |\vec{p}| + p_z \\ 0 \\ 0 \end{pmatrix}, \tag{B.2.8}$$

$$v(p,-) = \begin{pmatrix} \sqrt{p_0 - |\vec{p}|}\chi(p,+) \\ -\sqrt{p_0 + |\vec{p}|}\chi(p,+) \end{pmatrix} = \frac{-1}{\sqrt{|\vec{p}| + p_z}} \begin{pmatrix} 0 \\ 0 \\ |\vec{p}| + p_z \\ p_x + ip_y \end{pmatrix}, \tag{B.2.9}$$

We using the Spherical coordinates system for:

$$\mathbf{p} = -\mathbf{q}. \tag{B.2.10}$$

In this system, we have:

$$\begin{cases} p_x &= |\vec{p}| \sin\theta\cos\phi, \\ p_y &= |\vec{p}| \sin\theta\sin\phi, \\ p_z &= |\vec{p}| \cos\theta, \end{cases} \Longrightarrow \begin{cases} q_x &= -|\vec{p}| \sin\theta\cos\phi, \\ q_y &= -|\vec{p}| \sin\theta\sin\phi, \\ q_z &= -|\vec{p}| \cos\theta. \end{cases} \tag{B.2.11}$$

Then the fermion's spinors are:

$$u(p,+) = \frac{1}{\sqrt{|\vec{p}| + p_z}} \begin{pmatrix} 0 \\ 0 \\ |\vec{p}| + p_z \\ p_x + ip_y \end{pmatrix} = \frac{\sqrt{|\vec{p}|}}{\sqrt{1+\cos\theta}} \begin{pmatrix} 0 \\ 0 \\ 1 + \cos\theta \\ \sin\theta(\cos + i\sin\phi) \end{pmatrix}, \tag{B.2.12}$$

$$u(p,-) = \frac{1}{\sqrt{\sqrt{|\vec{p}|} + p_z}} \begin{pmatrix} -p_x + ip_y \\ |\vec{p}| + p_z \\ 0 \\ 0 \end{pmatrix} = \frac{|\vec{p}|}{\sqrt{1+\cos\theta}} \begin{pmatrix} \sin\theta(-\cos\phi + i\sin\phi) \\ 1 + \cos\theta \\ 0 \\ 0 \end{pmatrix}, \tag{B.2.13}$$

$$v(q,+) = \frac{-1}{\sqrt{|\vec{q}| + q_z}} \begin{pmatrix} -q_x + iq_y \\ |\vec{q}| + q_z \\ 0 \\ 0 \end{pmatrix} = \frac{-\sqrt{|\vec{p}|}}{\sqrt{1-\cos\theta}} \begin{pmatrix} \sin\theta(\cos\phi - i\sin\phi) \\ 1 - \cos\theta \\ 0 \\ 0 \end{pmatrix}, \tag{B.2.14}$$

$$v(q,-) = \frac{-1}{\sqrt{|\vec{q}|+q_z}} \begin{pmatrix} 0 \\ 0 \\ |\vec{q}|+q_z \\ q_x+iq_y \end{pmatrix} = \frac{-\sqrt{|\vec{p}|}}{\sqrt{1-\cos\theta}} \begin{pmatrix} 0 \\ 0 \\ 1-\cos\theta \\ -\sin\theta(\cos\phi+i\sin\phi) \end{pmatrix}. \tag{B.2.15}$$

Based on these forms of the spinor, we can easily do the numerical calcualtion due to the fact we can generate random events with a set of momentum.

B.3 Chisholm identity

Based on Ref. [14], we can transform our helicity amplitude into products of spinors such as the helicity amplitude could be written like a product $u\bar{u}$ with the possible insertion of γ^5's in the string. The different u, $\bar{u}$ in the string we have written have of course, in general, different arguments. Nonetheless one can turn each spinor product of two adjacent $\bar{u}u$, etc into a complex number written in terms of the momenta in our problem as we will see.

In the first step, for the momentum $\not{p}_i$ with $p_i^2 = m_i^2 = 0$ we use:

$$\not{p}_i = u(p_i,-)\bar{u}(p_i,-) + u(p_i,+)\bar{u}(p_i,+). \tag{B.3.16}$$

Then we can use the so-called Chisholm identity, which can be proved by the Dirac spinor:

$$\bar{u}(p,\lambda)\gamma_\mu u(q,\lambda)\gamma^\mu = 2\Big[u(p,-\lambda)\bar{u}(q,-\lambda) + u(q,\lambda)\bar{u}(p,\lambda)\Big]. \tag{B.3.17}$$

Appendix C

Monte Carlo method

C.1 Principles of Monte Carlo integration

By far the most common way to carry out phase space integration is the Monte Carlo method. This is due to following properties of Monte Carlo methods (Ref. [13]):

- Within the domain of application the rate of convergence is faster that that of other methods. The error decreases proportionally to $1/\sqrt{N}$ or even better, where N is the number of points at which the integrand is evaluated.
- The method is very general in the sense that it can be made reasonably efficient for all matrix elements occuring in practice.
- The method give many distributionat essentially the same expense as a single distribution; the same events need only be histogrammed in different ways.
- Monte Carlo computer programs can be made very simple for the general user.
- The Monte Carlo method treats events exactly as they are treated. The method thus resembles the way in which data are handled in experimental particle physics.

Now, consider a integral:

$$m = \int_0^1 dx f(x), \tag{C.1.1}$$

the Monte Carlo method give the mean of m is

$$\bar{m} = \frac{1}{N} \sum_{k=1}^{N} f(r_k). \tag{C.1.2}$$

The deviation of $\bar{m}$ from its most probable value is measured by the quantity:

$$\bar{\sigma}^2 = \frac{1}{N-1} \sum_{k=1}^{N} \Big[f(r_k) - \bar{m} \Big]^2. \tag{C.1.3}$$

The result of the Monte Carlo integration can thus be expressed as:

$$m = \bar{m} \pm \frac{\bar{\sigma}}{\sqrt{N}}. \tag{C.1.4}$$

C.2 Reduction of the statistical error

The statistical error of the crude Monte Carlo described above depends on two factors:

- The variance σ^2 of the function to be integrated.
- The number of randompoints at which the function is sampled.

The Monte Carlo method vecomes more efficient when the random points are generated so that their density is closer to $|f(x)|$. This method is called **importance sampling** (Ref. [13]). To apply it, we need a way to generater random numbers distributed according to a given density $g(x)$. The density $g(x)$ is defined so that the probability that a vaue between x and $x + dx$ is obtained is given by $(1/G)g(x)dx$ where $G = G(+\infty)$ and

$$G(x) = \int_{-\infty}^{x} d\tan(t). \tag{C.2.5}$$

Consider then the integral

$$I = \int_{x_{min}}^{x_{max}} dx f(x), \tag{C.2.6}$$

taking the new variable:

$$r = \frac{G(x) - G(x_{min})}{G(x_{max}) - G(x_{min})}, \tag{C.2.7}$$

which varies between 0 and 1 and has the differential

$$dr = \frac{g(x)dx}{G(x_{max}) - G(x_{min})}, \tag{C.2.8}$$

then we have the integral:

$$\begin{aligned} I &= \int_{x_{min}}^{x_{max}} dx f(x) \\ &= \int_{x_{min}}^{x_{max}} dx g(x) \frac{f(x)}{g(x)} \\ &= \Big[G(x_{max}) - G(x_{min})\Big] \int_0^1 dr \frac{f(x)}{g(x)}, \end{aligned} \tag{C.2.9}$$

where

$$x = G^{-1}\Big\{G(x_{min}) + r\Big[G(x_{max}) - G(x_{min})\Big]\Big\}. \tag{C.2.10}$$

For particle physics, we have the Breit-Wigner distribution:

$$g(x) = \frac{b^2}{(x-a)^2 + b^2}, \tag{C.2.11}$$

$$G(x) = \frac{\pi}{2} b + b \arctan \frac{x-a}{b}, \tag{C.2.12}$$

$$G^{-1}(y) = a + b \tan \frac{y - (\pi/2)b}{b}. \tag{C.2.13}$$

Bibliography

[1] D. J. Griffiths., *Introduction to Elementary Particles*.

[2] E. Conte, B. Fuks and G. Serret, *MadAnalysis 5, A User-Friendly Framework for Collider Phenomenology*, *Comput. Phys. Commun.* **184** (2013) 222–256, [1206.1599].

[3] M. E. Peskin and D. V. Schroeder, *An Introduction to quantum field theory*. Addison-Wesley Pub. Co, 1st ed., 1995.

[4] A. Denner, *Techniques for calculation of electroweak radiative corrections at the one loop level and results for W physics at LEP-200*, *Fortsch. Phys.* **41** (1993) 307–420, [0709.1075].

[5] M. Maggiore, *A Modern introduction to quantum field theory*. 2005.

[6] F. A. Berends, R. Pittau and R. Kleiss, *All electroweak four fermion processes in electron - positron collisions*, *Nucl. Phys.* (1994) 308–342, [hep-ph/9404313].

[7] H. M. Asatrian, A. Hovhannisyan and A. Yeghiazaryan, *The phase space analysis for three and four massive particles in final states*, *Phys. Rev.* **D86** (2012) 114023, [1210.7939].

[8] J. D. Bjorken and E. A. Paschos, *Inelastic Electron Proton and gamma Proton Scattering, and the Structure of the Nucleon*, *Phys. Rev.* **185** (1969) 1975–1982.

[9] A. Buckley, J. Ferrando, S. Lloyd, K. Nordström, B. Page, M. Rüfenacht et al., *LHAPDF6: parton density access in the LHC precision era*, *Eur. Phys. J.* **C75** (2015) 132, [1412.7420].

[10] Particle Data Group collaboration, M. Tanabashi, K. Hagiwara, K. Hikasa, K. Nakamura, Y. Sumino, F. Takahashi et al., *Review of particle physics*, *Phys. Rev. D* **98** (Aug, 2018) 030001.

[11] J. Baglio and N. Le Duc, *Fiducial polarization observables in hadronic WZ production: A next-to-leading order QCD+EW study*, *JHEP* **04** (2019) 065, [1810.11034].

[12] ATLAS collaboration, M. Aaboud et al., *Measurement of the $W^{\pm}Z$ boson pair-production cross section in pp collisions at $\sqrt{s} = 13$ TeV with the ATLAS Detector*, *Phys. Lett.* **B762** (2016) 1–22, [1606.04017].

[13] E. Byckling and K. Kajantie, *Particle Kinematics*. University of Jyvaskyla, Jyvaskyla, Finland, 1971.

[14] F. Boudjema and L. D. Ninh, *Leading Yukawa corrections to Higgs production associated with a tagged bottom anti-bottom pair in the standard model at the LHC*, *Phys. Rev.* **D77** (2008) 033003, [0711.2005].